Molecular Cell

Article

AKT constitutes a signal-promoted alternative exon-junction complex that regulates nonsense-mediated mRNA decay

Graphical abstract

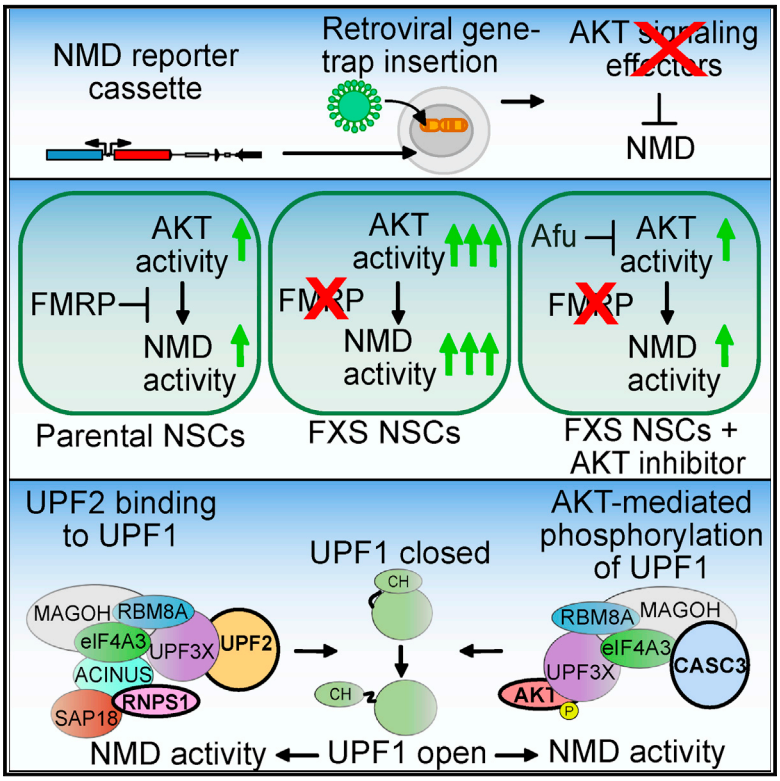

Highlights

- An unbiased genetic screen identifies effectors of AKT signaling as regulators of NMD
- AKT phosphorylation of UPF1 overcomes autoinhibition of UPF1 helicase activity
- AKT signaling promotes formation of EJCs containing AKT at the expense of UPF2
- AKT and UPF2 constitute alternative EJCs with distinct mechanisms of UPF1 activation

Authors

Hana Cho, Elizabeth T. Abshire, Maximilian W. Popp, Christoph Pröschel, Joshua L. Schwartz, Gene W. Yeo, Lynne E. Maquat

Correspondence

lynne_maquat@urmc.rochester.edu

In brief

Cho, Abshire, and coworkers demonstrate that the serine/threonine kinase AKT functionally replaces UPF2 in alternative EJCs that contain CASC3 and promotes NMD by phosphorylating UPF1. AKT-mediated NMD is stimulated by insulin. *FMR1*-KO NSCs treated with the AKT inhibitor Afuresertib manifest suppression of hyperactivated NMD, which typifies Fragile X syndrome.

Cho et al., 2022, Molecular Cell *82*, 1–18
August 4, 2022 © 2022 Elsevier Inc.
https://doi.org/10.1016/j.molcel.2022.05.013

CellPress

Please cite this article in press as: Cho et al., AKT constitutes a signal-promoted alternative exon-junction complex that regulates nonsense-mediated mRNA decay, Molecular Cell (2022), https://doi.org/10.1016/j.molcel.2022.05.013

Molecular Cell

CellPress

Article

AKT constitutes a signal-promoted alternative exon-junction complex that regulates nonsense-mediated mRNA decay

Hana Cho,[1,2,8] Elizabeth T. Abshire,[1,2,8] Maximilian W. Popp,[1,2] Christoph Pröschel,[3,4] Joshua L. Schwartz,[5,6,7] Gene W. Yeo,[5,6,7] and Lynne E. Maquat[1,2,9,*]

[1]Department of Biochemistry and Biophysics, School of Medicine and Dentistry, University of Rochester, Rochester, NY 14642, USA
[2]Center for RNA Biology, University of Rochester, Rochester, NY 14642, USA
[3]Department of Biomedical Genetics, School of Medicine and Dentistry, University of Rochester, Rochester, NY 14642, USA
[4]Stem Cell and Regenerative Medicine Institute, School of Medicine and Dentistry, University of Rochester, Rochester, NY 14642, USA
[5]Department of Cellular and Molecular Medicine, University of California, San Diego, La Jolla, CA, USA
[6]Stem Cell Program, University of California, San Diego, La Jolla, CA, USA
[7]Institute for Genomic Medicine, University of California, San Diego, La Jolla, CA, USA
[8]These authors contributed equally
[9]Lead contact
*Correspondence: lynne_maquat@urmc.rochester.edu
https://doi.org/10.1016/j.molcel.2022.05.013

SUMMARY

Despite a long appreciation for the role of nonsense-mediated mRNA decay (NMD) in destroying faulty, disease-causing mRNAs and maintaining normal, physiologic mRNA abundance, additional effectors that regulate NMD activity in mammalian cells continue to be identified. Here, we describe a haploid-cell genetic screen for NMD effectors that has unexpectedly identified 13 proteins constituting the AKT signaling pathway. We show that AKT supersedes UPF2 in exon-junction complexes (EJCs) that are devoid of RNPS1 but contain CASC3, defining an unanticipated insulin-stimulated EJC. Without altering UPF1 RNA binding or ATPase activity, AKT-mediated phosphorylation of the UPF1 CH domain at T151 augments UPF1 helicase activity, which is critical for NMD and also decreases the dependence of helicase activity on ATP. We demonstrate that upregulation of AKT signaling contributes to the hyperactivation of NMD that typifies Fragile X syndrome, as exemplified using *FMR1*-KO neural stem cells derived from induced pluripotent stem cells.

INTRODUCTION

Nonsense-mediated mRNA decay (NMD) is a cellular quality-control mechanism used to destroy aberrant mRNAs having the potential to encode toxic truncated proteins (Kishor et al., 2019; Kurosaki et al., 2019; Yi et al., 2021). During pre-mRNA splicing, the large macromolecular exon-junction complex (EJC) is deposited ~20–25-nts upstream of spliced exon-exon junctions. In what appear to be alternative EJCs, the eIF4A3, RBM8A, and MAGOH core EJC constituents are joined by either RNPS1, which recruits both UPF3X (also called UPF3B) and UPF2 NMD factors to trigger UPF2-dependent NMD, or, alternatively, CASC3, which recruits UPF3X but not UPF2 (Gehring et al., 2005; Gerbracht et al., 2020; Mabin et al., 2018). Although UPF2-independent NMD is known to occur (Gehring et al., 2005; Gong et al., 2009), given that UPF2 has the important function of transitioning UPF1 from a closed to open conformation (Clerici et al., 2009), what functionally replaces UPF2 in its absence has remained unknown. When at least one exon-exon junction resides >50–55-nts downstream of a premature termination codon (PTC), the terminating ribosome fails to remove the associated EJC, triggering NMD. Subsequently, the key ATP-dependent RNA helicase, UPF1, and its kinase, SMG1, assemble at the terminating ribosome and move to the EJC. SMG1 then hyperphosphorylates the N and C termini of UPF1. Hyperphosphorylated-UPF1 (p-UPF1) (1) inhibits further rounds of translation initiation (Isken et al., 2008), (2) recruits the endonuclease SMG6 and the SMG5-SMG7 complex, which recruits decapping and deadenylating activities to degrade the NMD target (Boehm et al., 2021; Chakrabarti et al., 2014; Loh et al., 2013), and (3) remodels the mRNP to resolve stalls in the degradative process (Franks et al., 2010; Lee et al., 2015).

Importantly, other physiological mRNA features, e.g., an unusually long and/or structured 3′ untranslated region (3′ UTR), an upstream open reading frame, some UGA selenocysteine-encoding codons, or alternative-splicing events, allow the cell to control ~10% of nonmutated cellular transcripts via NMD to better adapt to changing environments (Gardner, 2008, 2010; Jia et al., 2018; Karam et al., 2013; Kishor et al., 2019; Kurosaki et al., 2014; Nasif et al., 2018; Popp and Maquat, 2015; Wang et al., 2011; Yi et al., 2021; Zhu et al., 2020).

Please cite this article in press as: Cho et al., AKT constitutes a signal-promoted alternative exon-junction complex that regulates nonsense-mediated mRNA decay, Molecular Cell (2022), https://doi.org/10.1016/j.molcel.2022.05.013

The complexity of NMD is highlighted by recent discoveries of additional proteins that modulate NMD activity. For example, SMG8 and SMG9 inhibit the kinase activity of SMG1 (Yamashita et al., 2009). DExH-box helicase 34 (DHX34) and neuroblastoma amplified sequence (NBAS) coregulate NMD-sensitive transcripts (Anastasaki et al., 2011; Longman et al., 2013, 2020). Poly-pyrimidine tract-binding protein 1 (PTBP1) and heterogeneous nuclear ribonucleoprotein L (hnRNPL) each shield particular transcripts with long and/or structured 3′UTRs from NMD (Fritz et al., 2020; Ge et al., 2016; Kishor et al., 2019). In incompletely understood mechanisms, intracellular calcium levels, the unfolded protein response, and the general stress response each inhibit NMD (Gardner, 2008; Karam et al., 2013, 2015; Nickless et al., 2014; Wang et al., 2011). Additionally, certain developmental transitions require adjustment of NMD activity (Gong et al., 2009; Kurosaki et al., 2021a; Lou et al., 2016) and induction of apoptosis is associated with NMD attenuation (Jia et al., 2015; Popp and Maquat, 2015, 2018).

Genetic methods for identifying new mammalian NMD factors or cellular pathways that modulate NMD activity remain few. Two recent CRISPR-based screens combined with a highly engineered reporter system identified new regulators of 3′ UTR EJC-dependent NMD: vacuolar ATPase, which regulates processes required for function of the Fe–S cluster-containing ribosome recycling factor, ABCE1 (Zhu et al., 2020), and four others that have unclear roles in NMD (Alexandrov et al., 2017). Additionally, an siRNA-based screen identified ICE1, which facilitates anchoring of UPF3X to the EJC (Baird et al., 2018). Both screening methods are confined to preplanned gene targeting based on the design of reagents, i.e., guide RNAs or siRNAs.

Here, we adapt the unbiased targeting of a mutagen—a gene-trap retrovirus—to a haploid human-cell line (Blomen et al., 2015; Brockmann et al., 2017; Carette et al., 2009, 2010, 2011a, 2011b; Jae et al., 2013; Nieuwenhuis et al., 2017; Staring et al., 2017) that we have engineered to screen for effectors that enhance NMD activity. We identify 13 factors that constitute the AKT (i.e., protein kinase B) signaling pathway. Unexpectedly, we show that AKT constitutes an EJC that contains CASC3 but is devoid of RNPS1 and UPF2. As an EJC constituent, AKT functionally replaces UPF2 in NMD by phosphorylating UPF1 T151, thereby changing the cysteine-histidine (CH) domain from a closed "RNA clamping" conformation to an open conformation that favors helicase activity. In the absence of AKT, SMG1-mediated UPF1 phosphorylation is insufficient for the proper regulation of NMD. We also demonstrate that inhibiting hyperactivated AKT signaling that typifies Fragile X syndrome (Gross and Bassell, 2012; Gross et al., 2010; Jacquemont et al., 2018; Pellerin et al., 2016), the most common single-gene cause of autism, normalizes the enhanced decay of NMD targets in neural stem cells that lack the protein missing in FXS, FMRP.

RESULTS

Reporter design and delivery

We considered several important criteria when designing a reporter that accurately reflects the activity of NMD (Figure 1A). First, the reporter, which we call +(JC Intron), should have the necessary *cis*-residing information that renders it susceptible to NMD. In the case of 3′UTR EJC-mediated NMD, the intron should be located >50–55-nts downstream of a termination codon (Nagy and Maquat, 1998). Thus, we used a portion of the T cell receptor β (TCRβ) minigene transcript (Paillusson et al., 2005), including the intron between the joining J and constant C segments (JC Intron), considering that these sequences confer a >30-fold reduction in mRNA abundance by NMD (Gudikote and Wilkinson, 2002). Second, aiming to use fluorescence-activated single-cell sorting (FACS) to identify changes in NMD efficiency, we placed the coding region for a 3XFLAG-tagged mCherry protein upstream of the TCRβ minigene fragment so that translation terminates at the 3XFLAG-mCherry termination codon to produce 3XFLAG-mCherry fluorescence, trigger NMD, and preclude the production of protein containing traces of TCRβ. The latter is because HAP1 cells (Carette et al., 2011b) do not contain TCRα or TCRβ proteins. Thus, any unpaired TCRβ sequences expressed by our NMD reporter would result in reporter protein dislocation from the endoplasmic reticulum, followed by rapid degradation by the proteasome (Fiebiger et al., 2004), thereby limiting the sensitivity of our FACS-based assay. Finally, as a control, TCRβ sequences were flanked with Locus of X-over P1 (LoxP) sites, which are recognized by the Cre recombinase. As another control, we generated a version of our reporter that lacks only the JC intron, called Δ(JC intron), and is therefore immune to NMD (Figure 1A).

3XFLAG-mCherry NMD reporter gene transcription is driven by a bidirectional human cytomegalovirus immediate-early (CMV IE) promoter, with the NMD reporter in the antisense direction (see below). In the sense direction, we inserted sequences encoding the fluorescent HA-tagged mCerulean protein as an important internal control, e.g., for changes in cellular translation. To deliver these reporters to HAP1 cells as vesicular-stomatitis virus glycoprotein (VSV-G)-pseudotyped viral particles, these constructs were cloned into an HIV-1-based lentiviral vector so as to avoid mapping reporter integration sites after the mutagenesis step, which is mediated by integration of a murine stem cell virus-based gene-trap retrovirus. Cloning the intron-containing reporter in the antisense direction relative to the lentiviral long terminal repeats (LTRs) limits truncation of the viral genome (and the consequential low viral titers) during virus production. As compensation controls for FACS, we also generated single-color versions of our reporters, consisting of either the Δ(JC Intron) 3XFLAG-mCherry reporter or the HA-mCerulean reporter (Figure 1A). Transient transfection of human embryonic kidney (HEK)293T cells with these constructs showed that the 3XFLAG-mCherry NMD reporter protein was adequately expressed for biochemical analysis (Figure 1B) and FACS analysis (Figure 1C). Importantly, Δ(JC intron), which obviates NMD, yielded an ~10-fold increase in both protein and fluorescence (Figures 1B and 1C).

Reporter cell-line screening and validation

HAP1 cells were infected with lentiviral particles containing each of the four constructs (Figure 1A). Considering that the position of integration can affect construct expression, we screened monoclonal populations of infected HAP1 cells for a reporter

Please cite this article in press as: Cho et al., AKT constitutes a signal-promoted alternative exon-junction complex that regulates nonsense-mediated mRNA decay, Molecular Cell (2022), https://doi.org/10.1016/j.molcel.2022.05.013

CellPress

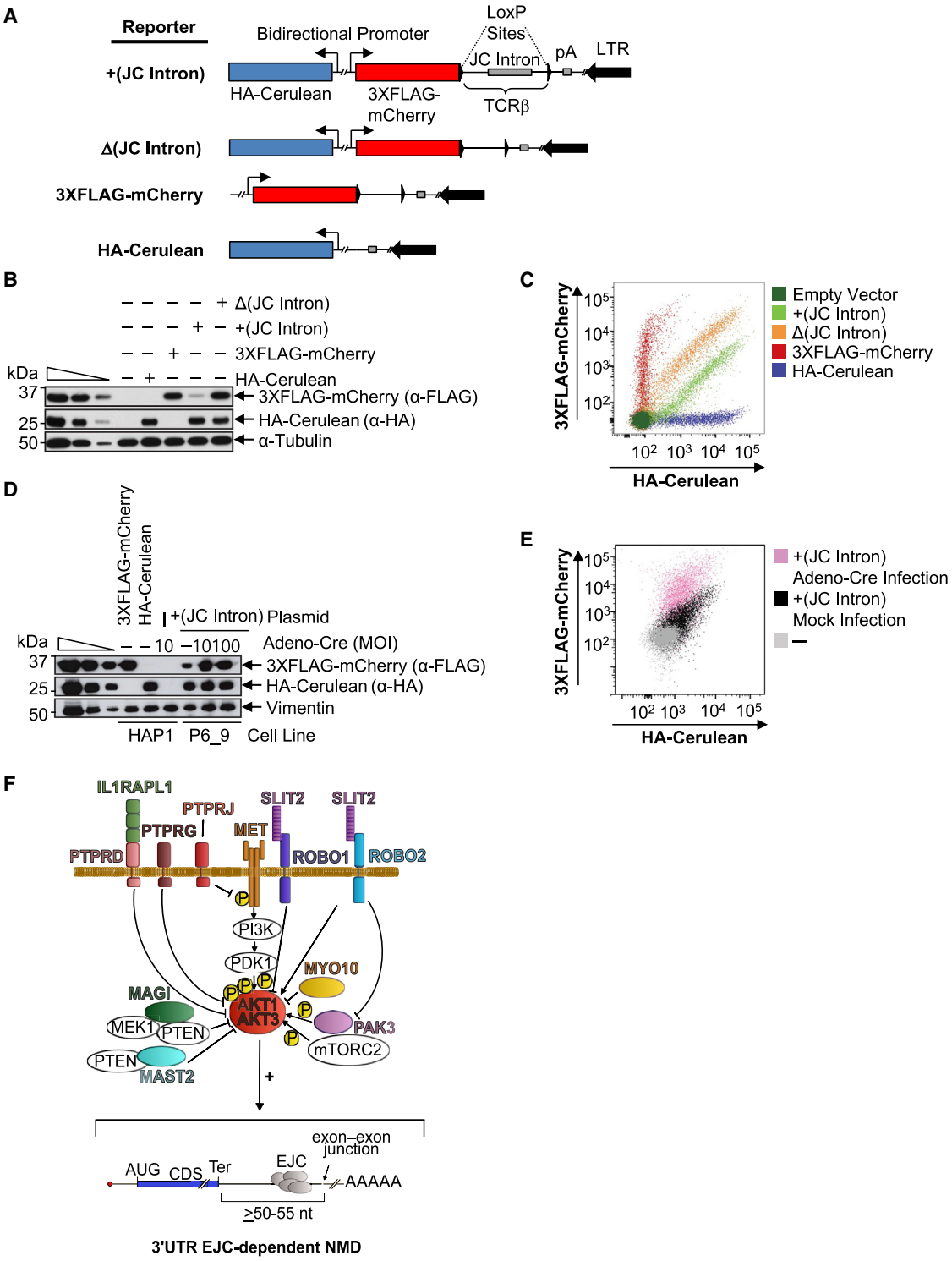

Figure 1. Haploid-cell screening identifies constituents of AKT signaling

(A) Diagram of reporter plasmids. Bidirectional promoter (↤↦), hCMV immediate-early promoter. Blue bar, control HA-mCerulean coding region in sense direction (↦) relative to viral replication. Red bar, 3XFLAG-mCherry coding region, fused to a TCRβ minigene and downstream SV40 polyadenylation sequence (pA). The 3XFLAG-mCherry translation termination codon resides 239-nts upstream of the JC intron, triggering NMD when translation terminates. LTR, lentiviral long terminal repeat. The Δ(JC Intron) reporter produces 3XFLAG-mCherry-TCRβ mRNA that is refractory to NMD when Cre mediates recombination via the LoxP sites (►). Control plasmids produce 3XFLAG-Cherry or HA-Cerulean, neither of which derives from an NMD target.

(legend continued on next page)

Please cite this article in press as: Cho et al., AKT constitutes a signal-promoted alternative exon-junction complex that regulates nonsense-mediated mRNA decay, Molecular Cell (2022), https://doi.org/10.1016/j.molcel.2022.05.013

cell line that satisfies two criteria: adequate 3XFLAG-mCherry fluorescence detectable by FACS and increased 3XFLAG-mCherry fluorescence when NMD is disrupted. Since HAP1 cells are difficult to transfect, to mimic the situation in the second criteria, we delivered Cre Adenovirus (Adeno-Cre) to monoclonal cell populations bearing the +(JC Intron) NMD reporter. This deletes the TCRβ sequences, including the JC intron, rendering the reporter transcript immune to NMD and also allowing individual monoclonal populations to be screened for cells showing an adequate increase in fluorescence. After one round of screening, Adeno-Cre-mediated deletion of the JC intron increased the amount of protein produced from the 3XFLAG-mCherry reporter in the HAP1 P6_9 cell line by 2.1-fold (Figure 1D). A second round of clonal isolation and screening was performed using these cells to arrive at our final reporter cell line, P6_9_E12 that, relative to mock infection, showed an ~10-fold increase in fluorescence by FACS upon Adeno-Cre-mediated deletion of the JC intron (Figure 1E).

As a mutagen, we used a gene-trap retrovirus containing a strong portable splice acceptor site (Carette et al., 2005), followed by the enhanced green fluorescent protein (eGFP) coding region and the SV40 polyadenylation site (Figure S1A). Gene-trap virus integration into genes encoding NMD *trans*-effectors will dampen NMD activity, leading to an increase in 3XFLAG-mCherry production and fluorescence, as mimicked by Δ(JC Intron) in our controls (Figure 1E). Thus, we isolated by FACS ~10 million cells representing ~1%–3% of cells with the highest 3XFLAG-mCherry expression in our mutagenized population (Figure S1B). These cells were expanded, and a second round of sorting, taking the top ~1%–3% of 3XFLAG-mCherry-expressing cells, was performed to further enrich for cells harboring insertions in genes encoding potential NMD effectors (Figure S1C).

With our selected cell population and our unselected mutagenized cell population, we identified gene-trap insertion sites using high-throughput sequencing (Brockmann et al., 2017). Data were processed using a pipeline at https://github.com/BrummelkampResearch. The number of unique disruptive insertions within each gene was tabulated for each cell population, as were the total number of disruptive insertions. The ratio of these two numbers provided a metric allowing comparison between populations for each gene using a one-sided Fisher's exact test. Potential NMD regulators were then ranked by p value after correcting p values for false discovery rates using the Benjamini-Hochberg procedure. The screen identified a number of potential NMD effectors that have not been shown previously to regulate NMD (Tables S1–S3). We were not surprised to see a dearth of the core NMD factors, many of which are essential proteins (Li et al., 2015; McIlwain et al., 2010; Medghalchi et al., 2001; Weischenfeldt et al., 2008), since our screening method requires several rounds of cell division, causing insertions that drastically decrease cellular fitness to be lost.

NMD effector verification

To verify potential NMD effectors, HEK293T cells were transiently transfected with either one of two control (CTL, i.e., non-targeting) siRNAs, *UPF1* siRNA, *SMG1* siRNA, or one of 45 siRNAs to downregulate 29 high p value ($-\log_{10}(\text{Pval}) > 20$) effectors. After 24 h, cells were transfected with a β-globin (Gl) test plasmid that was either Norm or Ter, the latter bearing a PTC that triggers NMD, and a mouse urinary protein (MUP) reference plasmid (Popp and Maquat, 2015). RT-qPCR analyses revealed that relative to each control siRNAs, one or more siRNAs to 20 candidate NMD effectors inhibited NMD (Figure S1D). Remarkably, 13 are constituents of the AKT signaling pathway, including AKT3 itself (Figure 1F; Table S4). Half-life studies using siRNA to each of four effectors chosen from the AKT pathway (i.e., ROBO1, ROBO2, SLIT2, and MYO10) confirmed that, relative to control siRNAs, downregulating each effector, like downregulating UPF1 or SMG1, stabilized a Gl NMD reporter mRNA after reporter gene transcription was shut-off using doxycycline (Figures S1E–S1L). Considering that AKT promotes cell survival by inactivating proapoptotic proteins (Duronio, 2008) and cells promote apoptosis by downregulating NMD via the caspase-mediated cleavage of UPF1 (Jia et al., 2015; Popp and Maquat, 2015), we pursued the idea that AKT signaling may promote NMD.

Evidence that AKT signaling promotes NMD

Although the mechanism remains unknown, NMD has been shown to be inhibited in HeLa cells transfected with pan-*AKT* siRNAs (Park et al., 2016) or, more recently, in HEK293FT cells treated with either AKT inhibitors from the GSK Kinase Inhibitor Set or *AKT1* gene deletion (Palma et al., 2021). In theory, AKT signaling could promote NMD by promoting mRNA export from the nucleus to the cytoplasm. However, RT-qPCR quantitations of the nuclear and cytoplasmic levels of *GAPDH* mRNA or FLAG-Gl Norm or Ter mRNA in the presence of CTL siRNA, *UPF1* siRNA, or siRNA to any of four proteins newly identified here as NMD effectors demonstrated that mRNA export was not altered (Figures S2A and S2B). In multiple experiments, performed in triplicate, downregulating each of seven AKT signaling effectors identified in the screen, including AKT3, and downregulating AKT1, AKT2, all three AKT proteins together or, as a positive control, UPF1 also inhibited the NMD of cellular NMD targets (Popp and Maquat, 2015), including *ATF3* mRNA (Figures 2A and 2B),

(B) Western blot of lysates of HEK293T cells transiently transfected with the specified plasmid using the specified antibody (α). Here and for every other western blot shown, leftmost lanes under the wedge consist of 3-fold dilutions of lysate and results represent two-three independent experiments. α-tubulin, loading control.

(C) FACS plot of cells from (B), transfected with specified plasmid. x axis, mCerulean fluorescence. y axis, mCherry fluorescence.

(D) Western blot of HAP1 cell lines, each stably expressing the indicated plasmid, before (−) or after infection with Adeno-Cre at the indicated MOI to delete TCRβ sequences, including the JC intron. HAP1 P6_9, cell line expressing +(JC Intron). Results represent three independent experiments.

(E) HAP1 P6_9_E12 reporter cells clonally isolated from P6_9 cells in (D) were then mock-infected (−) or infected with Adeno-Cre and analyzed by FACS. x and y axes, as in (C).

(F) Connection (+) between AKT signaling and NMD. Colored proteins are hits in the screen for NMD effectors. P, phosphate.

Please cite this article in press as: Cho et al., AKT constitutes a signal-promoted alternative exon-junction complex that regulates nonsense-mediated mRNA decay, Molecular Cell (2022), https://doi.org/10.1016/j.molcel.2022.05.013

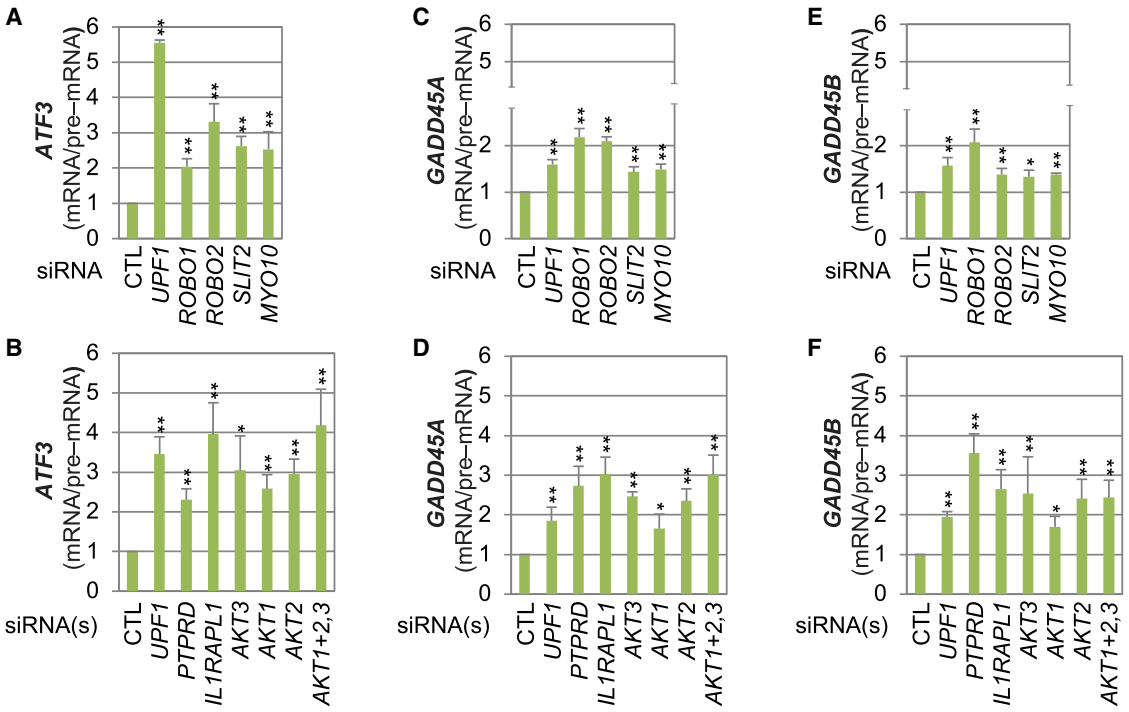

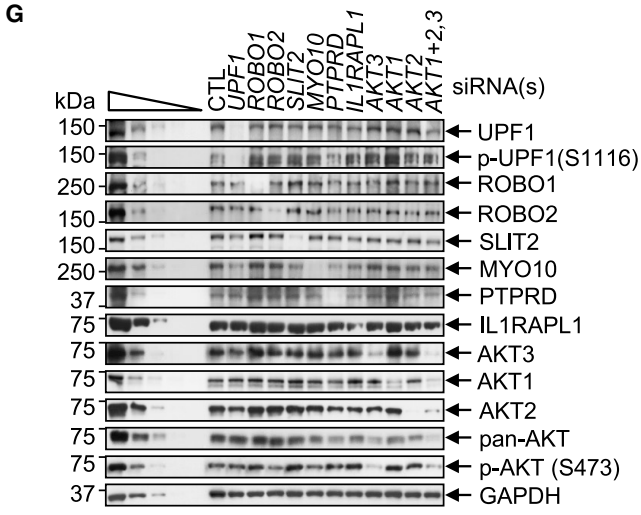

H

siRNA(s):	CTL	UPF1	ROBO1	ROBO2	SLIT2	MYO10	PTPRD	IL1RAPL1	AKT3	AKT1	AKT2	AKT1+2,3
Normalized to: GAPDH	1	0	2.0	1.5	2.1	1.7	0.8	1.9	1.7	1.9	1.2	1.9
Normalized to: UPF1	1	0.1	2.1	1.7	2.0	1.8	0.9	1.8	2.0	2.2	1.5	1.5

p-UPF1(S1116) levels

Figure 2. Downregulating constituents of the AKT pathway inhibits NMD

(A) Histograms of RT-qPCR of endogenous *ATF3* mRNA, normalized to the level of its pre-mRNA, using lysates of HEK293T cells transfected with the specified siRNA, and 24 h later, the MUP reference plasmid and either the FLAG-GI Norm and YFP-GPx1 Norm test plasmids or the FLAG-GI Ter and YFP-GPx1 Ter test plasmids. For each siRNA, the level of *ATF3* mRNA was normalized to the level of *ATF3* pre-mRNA and subsequently expressed relative to the normalized level in

(legend continued on next page)

Please cite this article in press as: Cho et al., AKT constitutes a signal-promoted alternative exon-junction complex that regulates nonsense-mediated mRNA decay, Molecular Cell (2022), https://doi.org/10.1016/j.molcel.2022.05.013

GADD45A mRNA (Figures 2C and 2D), and *GADD45B* mRNA (Figures 2E and 2F). Notably, *GADD45A* mRNA is targeted for NMD in a 3′ UTR EJC-independent mechanism, indicating that these effectors promote both 3′ UTR EJC-dependent NMD and the less-well characterized "long and/or structured 3′ UTR" NMD pathway. With the exception of *AKT2* siRNA for unknown reasons (see below), all siRNAs inhibited the NMD of both FLAG-Gl Ter mRNA (Figure S2C) and YFP-glutathione peroxidase 1 (GPx1) Ter reporter mRNA (Palma et al., 2021) (Figure S2D). We conclude that regulation of NMD is an overlapping function of AKT1, AKT2, and AKT3, at least for some NMD targets.

Although AKT proteins manifest many diverse functions that have been elucidated through multiple experimental approaches (Manning and Toker, 2017), our finding a role for AKT in NMD as an EJC constituent is unexpected. Notably, the inhibition of NMD upon downregulating AKT signaling effectors or AKT proteins is largely a consequence of effects on newly synthesized EJC-bound mRNAs (Ishigaki et al., 2001). Thus, although downregulating AKT signaling effectors or AKT proteins per se is known to inhibit steady-state translation (Ruggero and Sonenberg, 2005), what we are studying here reflects that AKT associates with newly synthesized cap-binding protein 80 (CBP80)-bound and not steady-state eIF4E-bound RNAs (see below).

Western blotting confirmed that each siRNA effectively downregulated its target protein (Figure 2G). Notably, none of the siRNAs to a constituent of the AKT pathway, with the exception of the *AKT* siRNAs, affected the level of AKT1, AKT2, or AKT3 and downregulating negative regulators of AKT signaling (i.e., SLIT2, MYO10, PTPRD, and ILIRAPL1), including AKT proteins themselves, increased the ratio of p-pan-AKT(S473) to pan-AKT (Figure 2G). p-AKT(S473) is the activated form of AKT that stabilizes phosphorylation at T308 and provides a measure of AKT activity (Manning and Toker, 2017). Our finding that NMD is inhibited by downregulating effectors that either promote or inhibit AKT indicates that just as it is the cycle of UPF1 phosphorylation and dephosphorylation at SMG1 target sites that is important for efficient NMD (Kurosaki et al., 2014), it is also the cycle of AKT-mediated phosphorylation and subsequent dephosphorylation (also of UPF1; see below) that is important for efficient NMD.

Each siRNA increased, or in the case of siRNA to *PTPRD* had no effect, on the level of UPF1 phosphorylation at S1116, i.e., p-UPF1(S1116), when normalized to either GAPDH or total-cell UPF1, with the expected exception of siRNA to *UPF1* itself (Figures 2G and 2H). To date, two kinases are known to phosphorylate UPF1: SMG1, which phosphorylates S1116 and other Ser/Thr residues in the N and C termini of UPF1 (Isken et al., 2008; Kashima et al., 2006; Kurosaki et al., 2014; Ohnishi et al., 2003; Yamashita et al., 2009), and ATM, which together with SMG1 contributes to stress-induced UPF1 phosphorylation at incompletely defined sites that include S1116 (Brumbaugh et al., 2004; Matsuoka et al., 2007). Given that siRNA to *AKT1*, *AKT2*, or *AKT3* also upregulated the level of p-UPF1(S1116), which has been used as a proxy for the efficiency of NMD (Kurosaki et al., 2021a and references therein), this proxy appears to be reliable only when AKT signaling is not inhibited.

Consistent with a role for AKT early in mRNA biogenesis, i.e., when NMD targets newly made mRNAs bound by CBP80 and EJCs, immunoprecipitations (IPs) of pan-AKT (hereafter referred simply as AKT) coimmunoprecipitated CBP80; EJC core constituents eIF4A3, RBM8A, and MAGOH; the peripheral EJC constituents CASC3 and UPF1; and the UPF1 kinase SMG1 in a partially RNase I-insensitive manner (Figure 3A). In keeping with the view that EJCs contain either CASC3 or RNPS1 and UPF2 (Gehring et al., 2005; Gerbracht et al., 2020; Mabin et al., 2018), neither RNPS1 nor UPF2 was detected in IPs of AKT (Figure 3A). Our finding that the peripheral EJC constituent UPF3X coimmunoprecipitated with AKT in an RNase I-resistant manner agrees with the report that UPF3X is required for AKT binding to an NMD target (Palma et al., 2021). To our knowledge, these results provide the first indication that AKT could be part of a UPF2- and RNPS1-devoid EJC, i.e., an alternative EJC, and raise the possibility that AKT may somehow functionally substitute for UPF2 to promote UPF1 helicase activity.

As expected, IPs of AKT immunoprecipitated activated p-AKT(S473) in an RNase I-insensitive manner (Figure 3A; hereafter, amino acids are numbered according to the AKT1 sequence, where AKT phosphorylation at T308 and S473 in AKT1 correspond, respectively, to T309 and S474 in AKT2 and T305 and S472 in AKT3). As controls, RNase I treatment precluded the coIP of poly(A)-binding protein C1 (PABPC1) with AKT, GAPDH failed to coimmunoprecipitate with AKT in the presence or absence of RNase I, and none of the assayed proteins were detected in IPs using rabbit (r)IgG (Figure 3A). Our finding that eIF4E1 failed to coimmunoprecipitate with AKT even in the absence of RNase I, but CBP80 did, indicates that AKT associates with newly made mRNAs prior to eIF4E1 replacement of CBP80 at the mRNA cap, i.e., before and/or during the pioneer round of translation (Ishigaki et al., 2001), as also noted by Palma et al. (2021). In fact, AKT, p-AKT(T308), and p-AKT(473) are each associated with intron-containing and partially spliced pre-mRNAs during the process of splicing (Figures S3B–S3D).

To confirm the importance of AKT signaling to NMD, HEK293T cells were cultured for 0, 30, 45, 60, and 120 min with 600 nM of

control (CTL) siRNA-treated cells, which was defined as 1. Here and below (i.e., B–F), results are means ± SD. n = 3. * $p < 0.05$; ** $p < 0.01$ by a two-tailed unpaired Student's t test.

(B) As in (A), but using the specified siRNAs.

(C) As in (A), but for *GADD45A* transcripts.

(D) As in (B), for *GADD45A* transcripts.

(E) As in (A), for *GADD45B* transcripts.

(F) As in (B), for *GADD45B* transcripts.

(G) Using lysates from (A) and (B), western blots. Results represent three independent experiments.

(H) Quantitation of the level of p-UPF1(S1116), normalized to the level of either UPF1 or GAPDH, each defined as 1 in the presence of CTL siRNA, determined using (G).

Please cite this article in press as: Cho et al., AKT constitutes a signal-promoted alternative exon-junction complex that regulates nonsense-mediated mRNA decay, Molecular Cell (2022), https://doi.org/10.1016/j.molcel.2022.05.013

CellPress

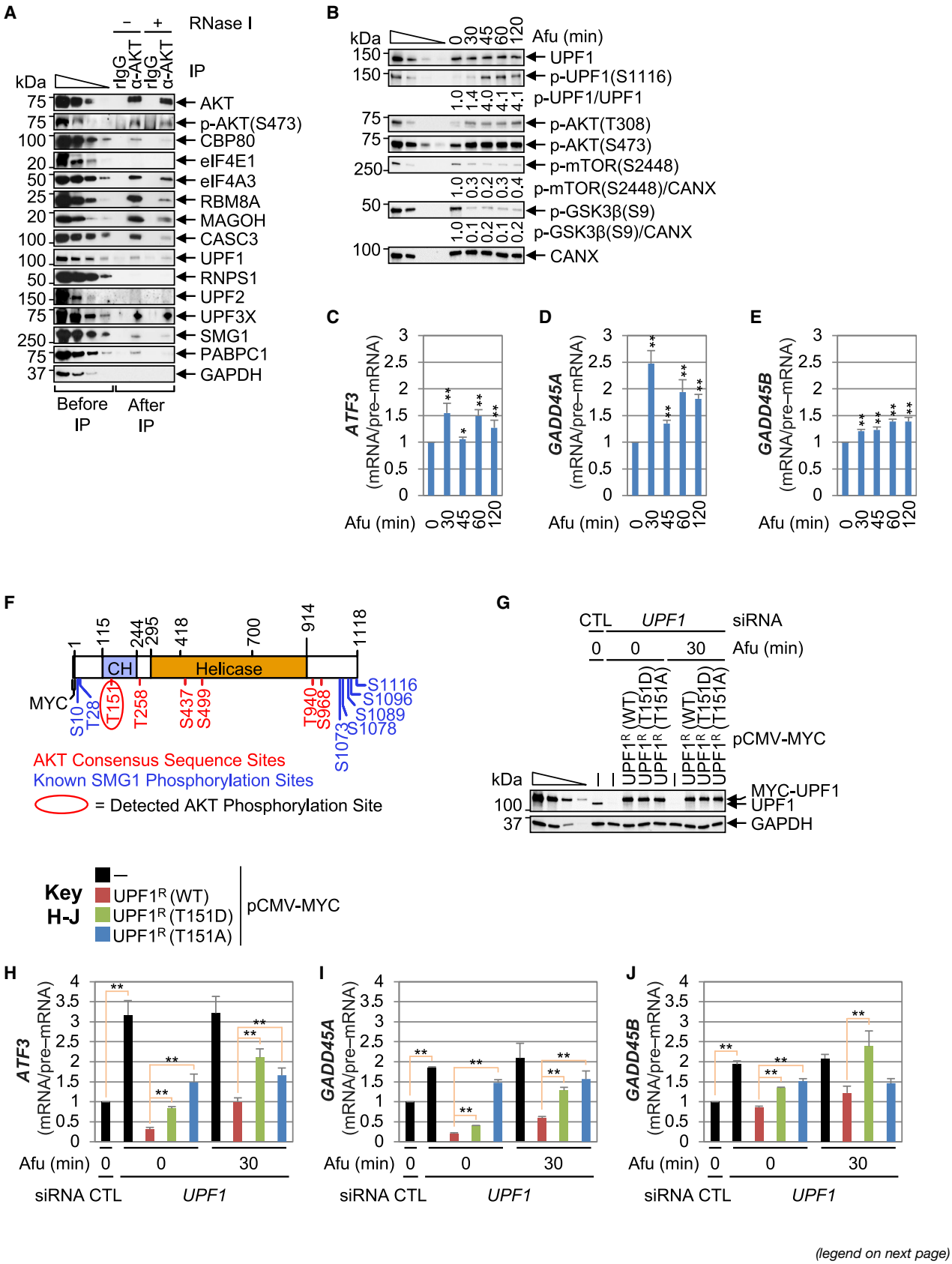

(legend on next page)

Please cite this article in press as: Cho et al., AKT constitutes a signal-promoted alternative exon-junction complex that regulates nonsense-mediated mRNA decay, Molecular Cell (2022), https://doi.org/10.1016/j.molcel.2022.05.013

the AKT catalytic inhibitor afuresertib (Afu), an anticancer drug that competes with ATP binding to p-AKT so as to inhibit the activity of p-AKT (Lin et al., 2012; Yamaji et al., 2017). We found that Afu indeed inhibited phosphorylation of the AKT targets p-mTOR(S2448) and p-GSK3β(S9) without inhibiting p-AKT(S473) (Nitulescu et al., 2016) (Figure 3B). Afu also inhibited the NMD of *ATF3*, *GADD45A*, and *GADD45B* mRNAs (Figures 3C–3E). These time points were chosen, given that longer incubation periods with Afu were accompanied by compensating signaling events that partially restored some degree of mTOR(S2448) and p-GSK3β(S9) phosphorylation (data not shown; Jansen et al., 2016) and NMD efficiency (data not shown). As is evidenced when comparing 0- to 30-min incubations with Afu (Figure 3B), our data are consistent with ATP-competitive AKT inhibitors, including Afu, inducing the level of p-AKT(T308) and p-AKT(S473) while inhibiting phosphorylation of AKT substrates (Vivanco et al., 2014; Yamaji et al., 2017). Afu also increased the level of p-UPF1(S1116) (Figure 3B), consistent with our finding that downregulating AKT increased the level of p-UPF1(S1116) (Figures 2G and 2H).

Evidence that AKT phosphorylates UPF1 at T151

Considering that our results are compatible with a direct role for AKT in NMD, we searched the PhosphoSitePlus database and found that UPF1 is phosphorylated at T151, which resides within the RXX(S/T) consensus sequence for AKT phosphorylation (Manning and Cantley, 2007; X denotes any amino acid, and either serine [S] or threonine [T] can be phosphorylated). There are an additional five S/T sites within UPF1 that reside within this consensus sequence: T258, S437, S499, T940, and S968 (Figure 3F). Of these, only T151 was detectably phosphorylated with high-confidence in mass spectrometry analyses of human UPF1 produced in and purified from baculovirus-infected Sf9 cells (Table S7). This was also true for human basal and luminal breast cancer xenografts and ovarian carcinoma tumors (Mertins et al., 2014) that, like many other cancers, are characterized by hyperactivated AKT signaling (Altomare and Testa, 2005).

In agreement with AKT-mediated phosphorylation at UPF1(T151), anti-MYC IPs of HEK293T-cell lysates expressing MYC-tagged UPF1 (MYC-UPF1) or, as a negative control, MYC alone demonstrated that MYC-UPF1, identified using anti-UPF1, reacted with anti-RXX(pS/pT) (Figure S3E). Moreover, reactivity was augmented after incubating cells for 30 min with 100 nM insulin (Figure S3E) to induce AKT signaling, as evidenced by increased levels of p-mTOR(S2448) and p-GSK3β(S9) (Figure S3F), as expected (Cross et al., 1995; Manning and Toker, 2017; Moschella et al., 2013).

AKT-mediated phosphorylation of UPF1 at T151 promotes NMD

To test for p-UPF1(T151) function in NMD, HEK293T cells were transfected with *UPF1* siRNA or CTL siRNA and subsequently with a MYC-UPF1 expression plasmid that produces siRNA-resistant (^{R}) mRNA encoding either MYC-UPF1^R wild type (WT), the phosphomimetic MYC-UPF1^R(T151D), the nonphosphorylatable MYC-UPF1(T151A) (Mookherjee et al., 2007), or, as a control, MYC alone. Cells transfected with *UPF1* siRNA either did not or did include 30-min incubations with Afu prior to lysis. *UPF1* siRNA reduced the abundance of cellular UPF1 to undetectable, each MYC-UPF1^R variant restored the level of cellular UPF1 to 2.2-fold to 3-fold above normal, and as expected, Afu treatment did not alter the level of either protein (Figure 3G). When compared with MYC-UPF1^R(WT), our finding that both MYC-UPF1^R(T151D) and MYC-UPF1^R(T151A) inhibited the NMD of *ATF3*, *GADD45A*, and *GADD45B* mRNAs (Figures 3H–3J) indicates that the cycle of UPF1 phosphorylation and dephosphorylation at T151 is critical for efficient NMD. Since Afu treatment further inhibited NMD when MYC-UPF1^R(WT) or MYC-UPF1^R(T151D) was expressed (Figures 3H–3J), T151 must not be the only site on UPF1 that undergoes AKT-mediated phosphorylation. Our finding that Afu had no additional effect on NMD when MYC-UPF1^R(T151A) was expressed (Figures 3H–3J) suggests that the one or more additional sites of AKT phosphorylation may require phosphorylation at T151.

AKT-mediated phosphorylation at T151 activates UPF1 helicase activity

Considering that T151 resides within a known UPF1 regulatory region (Kim and Maquat, 2019), we aimed to understand the consequence of T151 phosphorylation to UPF1 function. In theory, AKT-mediated phosphorylation of UPF1, like SMG1-mediated phosphorylation of UPF1, could promote NMD by via recruiting the SMG5−SMG7 heterodimer (Ohnishi et al., 2003). This, in turn, recruits the SMG6 endonuclease (Boehm et al., 2021) and the CCR4-NOT deadenylation complex (Chakrabarti et al., 2014; Loh et al., 2013) to initiate mRNA decay.

Figure 3. AKT, a constituent of CASC3-containing EJCs, phosphorylates UPF1 to activate NMD

(A) Western blot of lysates of HEK293T cells before (−) and after immunoprecipitation (IP) with α-AKT or, as a negative control, rabbit (r)IgG. IPs were in the absence (−) or presence (+) of RNase I. Results represent two independent experiments.

(B) Western blot of lysates of HEK293T cells cultured with 600 nM afuresertib (Afu) for the specified time. Results represent three independent experiments.

(C–E) Histograms of RT-qPCR of RNA deriving from lysates in (B), where efficiency of NMD was determined essentially as in Figure 2A, but the level of each mRNA/pre-mRNA in the absence of Afu was defined as 1. Here and below (i.e., H–J), results are means ± SD. n = 3. * $p < 0.05$; ** $p < 0.01$ by a two-tailed unpaired Student's t test.

(F) For UPF1, diagram of known SMG1-mediated phosphorylation sites (blue; Yamashita et al., 2001; Ohnishi et al., 2003; Kurosaki et al., 2014) and AKT consensus phosphorylation sites (red), of which T151 (red oval) was detected (Table S7).

(G) Western blot of lysates from HEK293T cells transfected with *UPF1* or CTL siRNA and, subsequently, a plasmid expressing MYC (−) or the specified siRNA-resistant (^{R}) MYC-UPF1. Cells were incubated with Afu for the denoted time prior to harvesting. GAPDH, loading control. Results represent three independent experiments.

(H) As in (C), but for samples analyzed in (G).

(I) As in (D), but for samples analyzed in (G).

(J) As in (E), but for samples analyzed in (G).

Please cite this article in press as: Cho et al., AKT constitutes a signal-promoted alternative exon-junction complex that regulates nonsense-mediated mRNA decay, Molecular Cell (2022), https://doi.org/10.1016/j.molcel.2022.05.013

CellPress

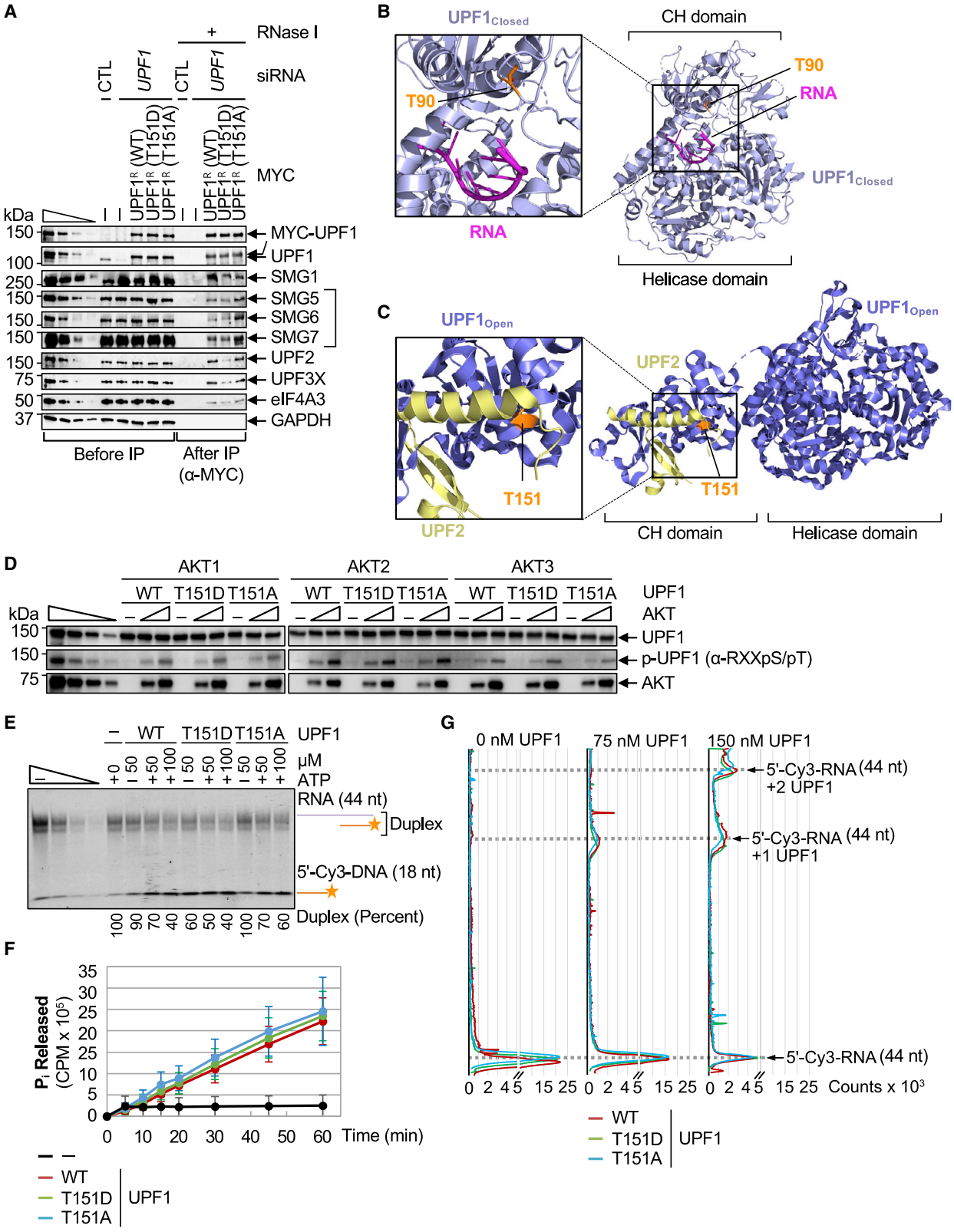

(legend on next page)

Please cite this article in press as: Cho et al., AKT constitutes a signal-promoted alternative exon-junction complex that regulates nonsense-mediated mRNA decay, Molecular Cell (2022), https://doi.org/10.1016/j.molcel.2022.05.013

SMG5-SMG7 and SMG6 coimmunoprecipitated with MYC-UPF1^R(WT) and MYC-UPF1^R(T151D) comparably but less efficiently than with MYC-UPF1^R(T151A) (Figure 4A, bracket), consistent with our finding that *AKT* siRNA upregulates the level of UPF1 phosphorylation at S1116 (Figures 2G and 2H) but inhibits NMD (Figures 3H–3J). This indicates that the enhanced and/or stabilized recruitment of SMG5-SMG7 and SMG6 without the ability of AKT to phosphorylate UPF1(T151) is insufficient to enhance NMD. However, recruitment of SMG5−SMG7 and SMG6 did not correlate with the coIP efficiency of SMG1: SMG1 coimmunoprecipitated more efficiently with MYC-UPF1^R(WT) than with either UPF1^R(T151D) or MYC-UPF1^R(T151A). Possibly, SMG1 binding to a substrate in the steady state does not provide a measure of kinase activity on that substrate or T151 phosphorylation status influences SMG1 binding.

We conclude that the inability to phosphorylate UPF1(T151A) or the inability to dephosphorylate UPF1 (T151D), despite the ability of UPF1(T151D) to promote helicase activity *in vitro* (see below), inhibits NMD. Our finding that UPF3X, eIF4A3, and CBP80 coimmunoprecipitate less efficiently with UPF1(T151D) than with UPF1(WT) or UPF1(T151A) (Figure 4A), suggests that once UPF1(T151) undergoes phosphorylation, then its augmented helicase activity releases it from the EJC, consistent with a reduced affinity of enzymes for their products (see below).

Alternatively or additionally to the recruitment of degradative activities, AKT-mediated phosphorylation of UPF1 could activate UPF1 ATPase and/or helicase activities, which are known to remodel NMD targets (Durand et al., 2016). These possibilities are appealing since AKT binding to UPF1 and/or AKT-mediated phosphorylation of UPF1(T151) may functionally replace UPF2, which is missing from AKT-containing EJCs (Figure 3A).

T151 resides within the CH domain of UPF1 (Figure 3F). Existing crystal structures of UPF1 suggest a mechanism by which UPF1 phosphorylation at T151 could promote NMD. When UPF1 is in the closed conformation (Figure 4B), the CH domain interacts in *cis* with the helicase domain, which inhibits UPF1 helicase and ATPase activities (Chamieh et al., 2008; Fiorini et al., 2013). UPF2 binding (Figure 4C) relieves autoinhibition of the CH domain by causing a conformational shift that displaces the CH domain from its contact with the helicase domain so as to promote RNA-dependent helicase activity while loosening RNA binding (Chakrabarti et al., 2011; Gowravaram et al., 2018).

Clues to T151 function in human UPF1 might derive from studies of the corresponding amino acid, T90, in *Saccharomyces cerevisiae* UPF1, since the structures of human and *S. cerevisiae* UPF1 are highly conserved (Figure S4A). Consistent with the possibility of p-T151 promoting UPF1 helicase activity, T90 in the closed "RNA clamping" conformation of *S. cerevisiae* UPF1 is pointed down toward (but not contacting) the helicase domain where RNA is bound. Thus, it is possible that p-T151 in human UPF1, by placing a negatively charged phosphate group in proximity to negatively charged RNA, could weaken the CH domain-helicase domain interaction to promote the open conformation and ATPase and helicase activities. Consistent with this possibility, UPF2, UPF3X, and eIF4A3 coimmunoprecipitated less efficiently with MYC-UPF1^R(T151D) than with MYC-UPF1^R(WT) or MYC-UPF1^R(T151A) (Figure 4A).

To test this hypothesis, human UPF1 variants consisting of UPF1 amino acids 115–914 (Figure S4B) were purified from *E. coli* and used in *in vitro* kinase assays. Probing for phosphorylation of UPF1 at AKT consensus sequences using α-RXX(pS/pT) demonstrated that incubations with increasing concentrations of AKT1, AKT2, or AKT3 resulted in a dose-dependent but paralog-specific reactivity of UPF1 WT, T151D, and T151A with α-RXX(pS/pT) (Figure 4D). This was despite each AKT paralog phosphorylating the GSK3β(S9) consensus sequence with comparable efficiencies (Figures S4C and S4D). Notably, phosphorylation of UPF1 by each paralog at one or more of the three additional AKT consensus sequences within amino acids 115–914 (Figure 3F) must not depend on phosphorylation of UPF1 T151, at least *in vitro* (Figure 4D).

In modified helicase activity assays (Chakrabarti et al., 2011; Kurosaki et al., 2014), UPF1 T151D was found to release 5′ Cy3-labeled DNA from base-pairing with the 3′ end of a 44-nt RNA more efficiently than does either UPF1 WT or T151A (Figure 4E). This suggests that AKT-mediated phosphorylation of UPF1 at T151 changes CH domain conformation to promote UPF1 helicase activity. Relative to UPF1 WT or T151A, the unwinding activity of UPF1 T151D was less dependent on ATP (Figure 4E) despite all three proteins manifesting comparable ATPase activity (Figure 4F) that was unaffected when AKT1

Figure 4. AKT-mediated UPF1 phosphorylation at T151 promotes UPF1 helicase activity

(A) Western blot of lysates of HEK293T cells transiently transfected with the denoted siRNA and the MYC (−) or specified MYC-UPF1^R expression vector. Results represent two independent experiments.

(B) Rendering of *S. cerevisiae* UPF1 (light blue) in complex with RNA (magenta) in the closed conformation (PDB: 2XZL; Chakrabarti et al., 2011). Note that T90 (orange) corresponds to human UPF1 T151 (orange). The proximity of T90 to RNA is detailed to the right. See Figure S4A for superimposition of human UPF1 in the closed conformation (PDB: 2XZO; Chakrabarti et al., 2011), which lacks T151, on this rendering of *S. cerevisiae* UPF1.

(C) Rendering of the open configuration of human UPF1 (dark blue) in complex with a fragment of UPF2 (yellow) (PDB: 2WJV; Clerici et al., 2009). T151 in the open CH domain is detailed to the right.

(D) Western blot of *in vitro* kinase assays, where phosphorylation of the specified UPF1(115–914) variant by increasing amounts of the denoted AKT paralog is detected using α-RXX(pS/pT). Results represent three independent experiments.

(E) In-gel fluorescence quantitation of duplex remaining, calculated as a percent of input, which is defined as 100, after increasing amounts of the specified UPF1(115–914) are incubated *in vitro* in the absence (−) or presence (+) of ATP with a 5′ Cy3-labeled 18 nt-DNA duplexed to a 44-nt RNA. Gold star, Cy3. Results represent three independent experiments.

(F) ATPase assays of the specified UPF1(115–914) variant, quantitated as released ^{32}[P], i.e., inorganic phosphate (Pi), from γ^{32}[P]-ATP as a function of incubation time. Results represent three independent experiments.

(G) Quantitations, using increasing concentrations (0, 75, and 150 nM) of the specified UPF1(115–914) variant, of UPF1 binding to a 5′ Cy3-labeled 44-nt RNA. Results represent three independent experiments.

Please cite this article in press as: Cho et al., AKT constitutes a signal-promoted alternative exon-junction complex that regulates nonsense-mediated mRNA decay, Molecular Cell (2022), https://doi.org/10.1016/j.molcel.2022.05.013

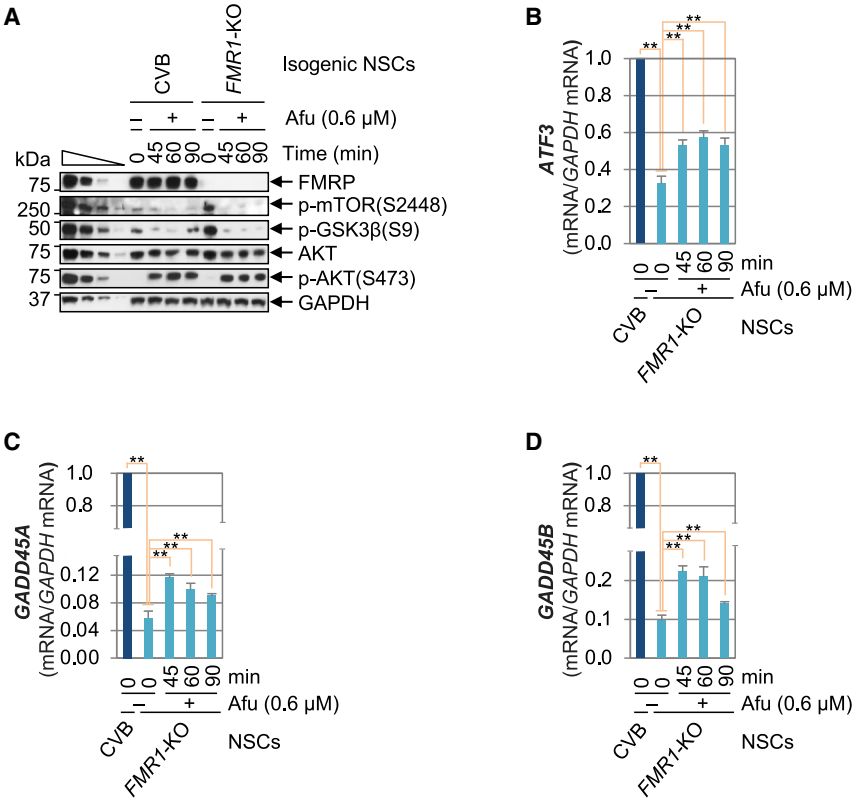

Figure 5. Hyperactivated AKT signaling contributes to hyperactivated NMD in human *FMR1*-KO NSCs

(A) Western blot of lysates of control (CVB) and isogenic *FMR1*-KO NSCs generated from the corresponding iPSCs and then cultured for the specified time in the absence (–) or presence (+) of 600 nM Afu. Results represent three independent experiments.

(B) Histograms of RT-qPCR results essentially as in Figure 3C, but normalizations of *ATF3* mRNA are to *GAPDH* mRNA. Here and below (C and D), results are means ± SD. n = 3. * $p < 0.05$; ** $p < 0.01$ by a two-tailed unpaired Student's t test.

(C) As in (B), but for *GADD45A* mRNA.

(D) As in (B), but for *GADD45B* mRNA.

was added to reactions (data not shown). RNA-binding activity was also not significantly different between the three UPF1 proteins (Figures 4G and S4E).

We conclude that analogously to how UPF2 binding to the UPF1 CH domain (Figure 4C) relieves autoinhibition by displacing the CH domain from its contact with the helicase domain so as to promote ATP-dependent helicase activity, AKT-mediated phosphorylation of T151 does likewise. However, like STAU binding to the UPF1 CH domain (Park et al., 2013), AKT binding augments helicase activity per ATP cleaved.

Dampening AKT signaling counters hyperactivated NMD attributable to FMRP loss

FXS, the most common single-gene cause of intellectual disability and autism, is attributable to the lack of FMRP (Malecki et al., 2020; Razak et al., 2020; Suardi and Haddad, 2020). We have shown that induced pluripotent stem cells (iPSCs) developed from FXS-patient fibroblasts exhibit abnormally enhanced decay of NMD targets (Kurosaki et al., 2021a). The mechanism is at least two-fold: the absence of FMRP, which is a translational repressor that is recruited to and/or stabilized on NMD targets by p-UPF1 and/or UPF1, can lead to the increased decay and/or hypertranslation of NMD targets; and a cohort of NMD factor-encoding mRNAs, which are NMD targets themselves, are "translationally buffered-up" to produce abnormally high levels of protein despite their abnormally reduced abundance, resulting in increased decay (Kurosaki et al., 2021a).

AKT signaling is abnormally enhanced in FXS patients (Gross and Bassell, 2012; Gross et al., 2010; Jacquemont et al., 2018; Pellerin et al., 2016), leading us to assess the physiological relevance of upregulated AKT signaling to the hyperactivated decay of NMD targets in FXS. Considering difficulties in parsing out cause-and-effect(s) using FXS patient-derived cells due to heterogeneity between FXS patients, we derived neural stem cells (NSCs) from syngeneic iPSCs: the control CVB iPSC line was used to generate an *FMR1*-KO iPSC counterpart (Figures S5A–S5H). CVB-derived NSCs cultured in the absence or presence of 600 nM Afu for 0, 45, 60, and 90 min demonstrated that Afu-mediated inhibition of AKT signaling, as measured by decreased levels of p-mTOR(S2448) and p-GSK3β(S9), was evident by 30 min and had rebounded by 90 min (Figure 5A). In RT-qPCR assays, NMD was indeed hyperactivated in *FMR1*-KO NSCs relative to parental CVB-derived NCSs in the absence of Afu, i.e., at time 0, and NMD was subsequently attenuated when Afu was used to inhibit AKT signaling in *FMR1*-KO NSCs (Figures 5B–5D). Thus, the observed hyperactivated NMD that typifies the loss of FMRP in FXS (Kurosaki et al., 2021a, 2021b) appears to be partially attributable to enhanced AKT signaling.

Additional evidence that AKT and UPF2 constitute alternative EJCs

Our findings that phosphorylation of UPF1 at T151 and UPF2 function analogously to promote UPF1 activity during NMD and that UPF2, unlike UPF3X, fails to coimmunoprecipitate with AKT (Figures 3 and 4), suggest that AKT may constitute what has been called the UPF2-independent branch of NMD (reviewed in Yi et al., 2021). We showed years ago that UPF2-independent NMD is augmented during myogenesis, when UPF2 levels decrease so as to decrease what we called "classical" or UPF2- and UPF3X-dependent NMD (Gong et al., 2009). Consistent with a possible role of AKT in UPF2-independent NMD, it was since well established that AKT signaling promotes myogenesis (Dörpholz et al., 2017). We questioned if downregulating UPF2 might augment the formation of AKT-containing EJCs, whereas downregulating AKT1, 2, and 3 might augment the formation UPF2-containing EJCs. This possibility required testing

Please cite this article in press as: Cho et al., AKT constitutes a signal-promoted alternative exon-junction complex that regulates nonsense-mediated mRNA decay, Molecular Cell (2022), https://doi.org/10.1016/j.molcel.2022.05.013

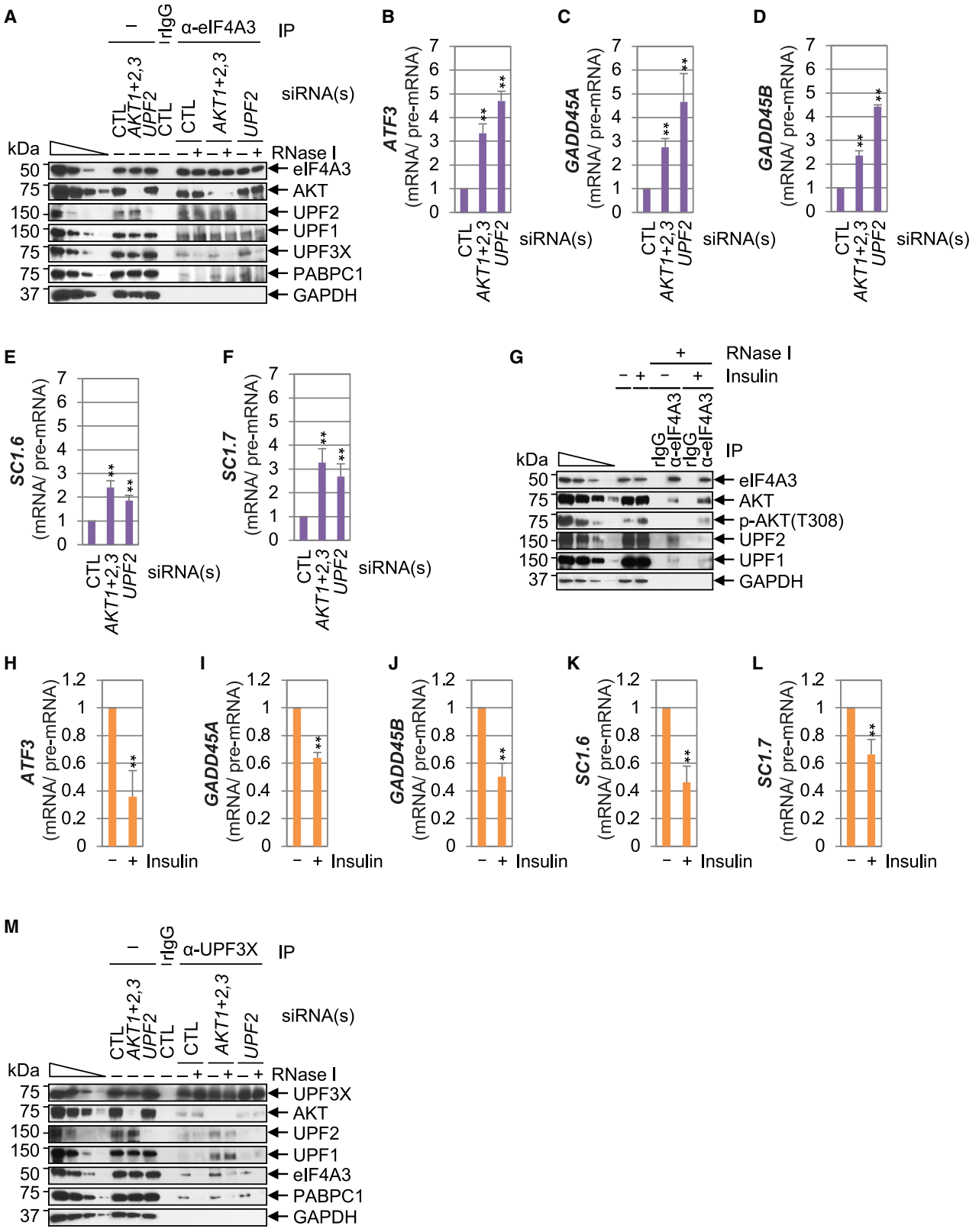

(legend on next page)

Please cite this article in press as: Cho et al., AKT constitutes a signal-promoted alternative exon-junction complex that regulates nonsense-mediated mRNA decay, Molecular Cell (2022), https://doi.org/10.1016/j.molcel.2022.05.013

considering the proposal that RNPS1- and UPF2-containing EJCs are precursors to CASC3-containing EJCs (Mabin et al., 2018).

Using IPs of eIF4A3 as an assay for EJC constituents, downregulating AKT did not increase the coIP of UPF2 and downregulating UPF2 did not increase the coIP of AKT (Figure 6A), suggesting that an obligate precursor-product relationship between UPF2-containing EJCs and AKT-containing EJCs does not exist. This finding also suggests that AKT binding to an EJC is a regulated process, possibly enhanced by AKT signaling. Notably, the NMD of *ATF3*, *GADD45A*, and *GADD45B* mRNAs was inhibited upon downregulating either all three AKTs or UPF2 (Figures 6B–6D), indicating that both AKT- and UPF2-mediated pathways were active either on the same molecule and/or different molecules of the three mRNAs. We draw the same conclusion from our finding that *AKT* siRNAs as well as *UPF2* siRNA inhibit the NMD of *SC1.6* and *SC1.7* mRNAs, which are splice isoforms of *SRSF2* mRNA whose NMD is, respectively, 3′ UTR EJC-independent or also due to a single 3′ UTR EJC that follows the 50–55-nt rule (Figures 6E and 6F).

In agreement with AKT signaling augmenting AKT-mediated NMD, repeating the eIF4A3 IPs using cells in which AKT signaling was enhanced by insulin treatment after serum deprivation, increased the coIP of AKT, and decreased the coIP of UPF2 (Figure 6G), while promoting NMD efficiency (Figures 6H–6L). Consistent with AKT and UPF2 binding to either overlapping or mutually exclusive regions of UPF3X, IPs of UPF3X demonstrated that downregulating AKT upregulated the coIP of UPF2 and downregulating UPF2 upregulated the coIP of AKT (Figure 6M).

DISCUSSION

Here, we develop a haploid-cell genetic screen in search of yet-to-be defined NMD effectors and report that 13 effectors that were identified in the screen constitute the AKT signaling pathway (Figures 1, 2, and S1). Eight additional lines of evidence confirm that AKT signaling promotes NMD by forming an alternative AKT-containing EJC. (1) Downregulating AKT1, AKT2, and AKT3 individually or together inhibits the NMD of reporter and cellular NMD targets in human cells (Figures 2, S1, and S2). (2) IPs of AKT and p-AKT from human-cell lysates indicate that AKT forms an RNase I-resistant complex with UPF1 and EJC constituents eIF4A3, RBM8A, MAGOH, and CASC3 on mRNAs bound by CBP80, but not eIF4E1, consistent with a direct effect on CBP80–CBP20-bound and, when present, EJC-bound mRNAs, which are targeted for NMD (Figure 3). (3) LC/MS-MS revealed that human UPF1 is phosphorylated at T151, which resides within the CH domain at an AKT consensus sequence (Figure 3). (4) Activation of cellular AKT activity by insulin augments the reactivity of UPF1 with anti-RXX(pS/pT), which is the phosphorylated consensus sequence for AKT (Figure S3). (5) Replacing cellular UPF1 with either the T151D phosphomimetic variant of UPF1 or the T151A variant that cannot be phosphorylated at T151 inhibits NMD, consistent with efficient NMD requiring cycles of AKT-mediated UPF1 phosphorylation followed by dephosphorylation at T151 (Figure 3). (6) In *in vitro* assays (Figure 4), relative to UPF1 WT and UPF1 T151D manifests increased helicase activity without increased ATPase activity, whereas UPF1 T151A behaves more like UPF1 WT. This explains how UPF2-devoid EJCs can trigger NMD: AKT functionally substitutes for UPF2 by opening the autoinhibited CH domain of UPF1 to promote efficient NMD. (7) Inhibiting AKT signaling in *FMR1*-KO NSCs dampens the hyperactivated NMD that we show typifies these NSCs (Figure 5), consistent with inhibiting PI3K signaling, which functions upstream of AKT, normalizing the FXS phenotype (Kang et al., 2021). (8) An increase in AKT-containing EJCs, and a concomitant decrease in UPF2-containing EJCs, can be achieved by augmenting cellular AKT signaling using insulin (Figure 6). AKT function as an EJC constituent may be accompanied by its other roles that, e.g., result in CBP80 phosphorylation by S6 kinase, thereby stimulating the cap-binding activity of the CBC (Wilson et al., 2000).

We conclude that AKT function in NMD is a regulated process. That noted, our finding that *SC1.7* mRNA, which is an NMD target because of a single 3′ UTR EJC, can be targeted in either a UPF2-dependent or AKT-dependent mechanism indicates that at least some conditions allow for both mechanisms to function and, e.g., different *SC1.7* molecules to harbor either a UPF2- and RNPS1-containing EJC or a AKT- and CASC3-containing EJC (Figure 6).

We demonstrate that NMD is activated by AKT-mediated UPF1 phosphorylation that most likely works together with SMG1-mediated UPF1 phosphorylation for at least three reasons. For one, Park et al. (2016) observed increased NMD efficiency in HeLa cells exposed for 4 h to insulin, which promotes AKT signaling, without altering the level of p-UPF1(S1096), which like p-UPF1(S1116), is catalyzed by SMG1. For another, although SMG1-mediated UPF1 phosphorylation recruits either directly or indirectly mRNA degradative activities, whether AKT-mediated phosphorylation at UPF1 T151 does likewise is uncertain. For a third, CASC3, which defines AKT-containing EJCs, promotes SMG6 endonuclease-mediated cleavage of NMD targets (Gerbracht et al., 2020), if not also the SMG5–SMG7-mediated recruitment of other mRNA decay factors to NMD targets, consistent with the partial RNase I-insensitive coIP of SMG1 with AKT (Figure 3A).

Figure 6. Additional evidence that AKT and UPF2 constitute alternative EJCs

(A) Western blot of lysates of HEK293T cells transfected with the specified siRNA(s) before or after IP using α-eIF4A3, or as a control rIgG, in the presence (+) or absence of RNase I. Results represent two independent experiments.

(B–D) Histograms of RT-qPCR of RNA deriving from lysates analyzed in (A) prior to IP, as in Figures 2A–2F. Here and below (i.e., E, F, and H–L), results are means ± SD. n = 3. * $p < 0.05$; ** $p < 0.01$ by a two-tailed unpaired Student's t test.

(E and F) Histograms of RT-qPCR of RNA deriving from lysates analyzed in (A) prior to IP, but for *SC1.6* and *SC1.7* mRNA/pre-mRNA.

(G) Western blot of lysates of HEK293T cells that were serum-deprived and subsequently incubated in the presence (+) or absence of insulin before or after IP with α-eIF4A3 or rIgG. Results represent two independent experiments.

(H–J) As in (B)–(D), using RNA from lysates analyzed in (G).

(K and L) As in (E) and (F), using RNA from lysates analyzed in (G).

(M) As in (A), but for α-UPF3X IPs. Results represent two independent experiments.

Please cite this article in press as: Cho et al., AKT constitutes a signal-promoted alternative exon-junction complex that regulates nonsense-mediated mRNA decay, Molecular Cell (2022), https://doi.org/10.1016/j.molcel.2022.05.013

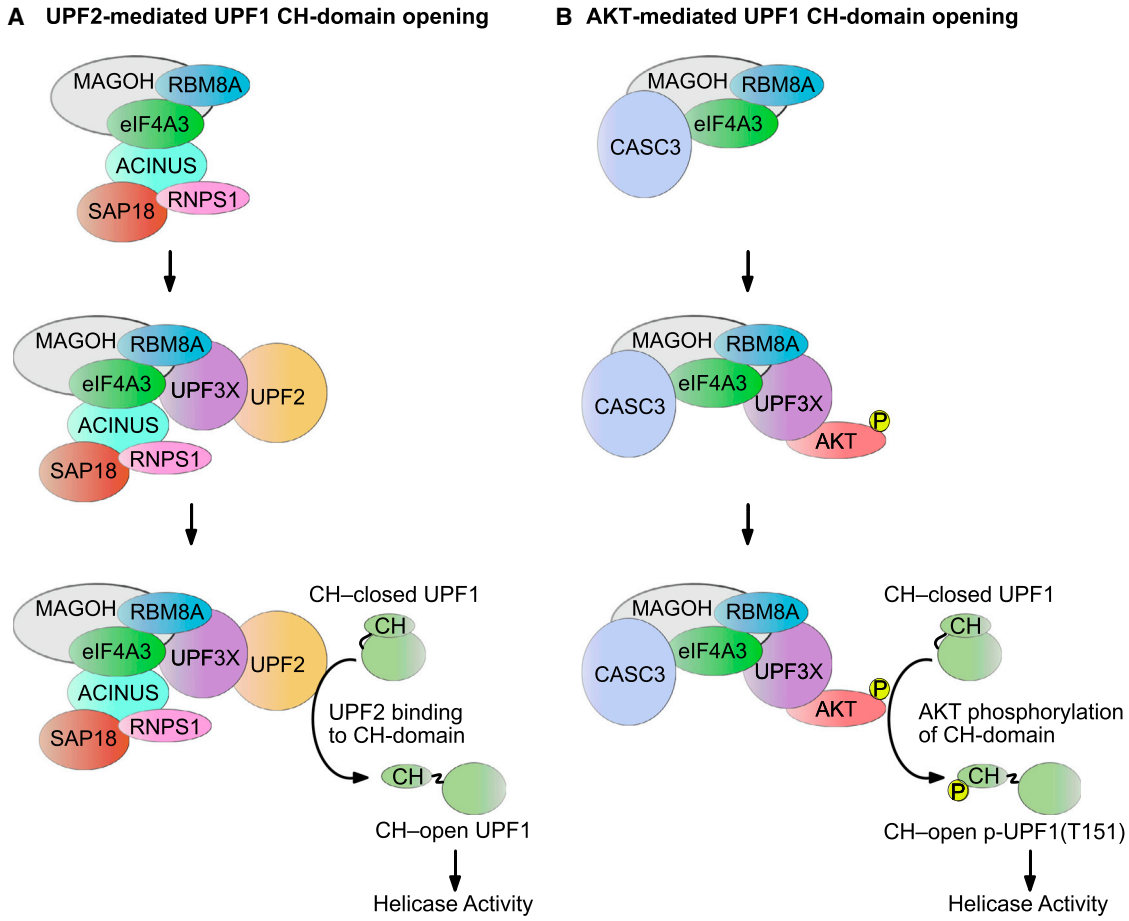

Figure 7. Model for UPF2-mediated NMD and AKT-mediated NMD

(A) EJC-associated UPF2, which typifies an RNPS1-containing EJC, binds to the CH domain of UPF1 to overcome UPF1 autoinhibition, thereby promoting UPF1 helicase activity and NMD.

(B) EJC-associated AKT, which typifies a CASC3-containing EJC, phosphorylates T151 in the CH domain of UPF1 to overcome UPF1 autoinhibition, thereby promoting UPF1 helicase activity and NMD.

Our data explain how UPF1 can function in NMD independently of UPF2 (Figure 7). In the context of 3′ UTR EJC-dependent NMD, it is either UPF2 or AKT that is recruited to an EJC by UPF3X. It has been assumed that UPF3X binds to EJCs prior to UPF2 (Schlautmann and Gehring, 2020). However, we cannot distinguish between the possibility that EJC-associated UPF3X recruits UPF2 or AKT and the possibility that UPF3X joins the EJC together with UPF2 or AKT. This is because UPF2 and UPF3X can form a complex that is independent of the EJC, as is evident by competition between UPF2 and AKT for coIP with UPF3X but the lack of competition between UPF2 and AKT for coIP with eIF4A3 (Figure 6).

Our study offers unanticipated insight into the importance and complexity of cellular pathways that regulate mammalian-cell NMD.

Limitations of the study

Our screen will miss NMD factors that are required for cell proliferation. Sites of AKT mediated phosphorylation in addition to T151 exist on UPF1 but remain to be mapped. In addition to Fragile X syndrome, certain cancers for which the anticancer drug Afu is in clinical trials, and insulin signaling, there will be many yet-to-be defined conditions under which AKT signaling promotes NMD.

STAR★METHODS

Detailed methods are provided in the online version of this paper and include the following:

- KEY RESOURCES TABLE
- RESOURCE AVAILABILITY
  - Lead contact
  - Materials availability
  - Data and code availability
- EXPERIMENTAL MODEL AND SUBJECT DETAILS
  - Cell lines
- METHOD DETAILS
  - Plasmid constructions
  - Cells and cell culture for the haploid genetic screen

Please cite this article in press as: Cho et al., AKT constitutes a signal-promoted alternative exon-junction complex that regulates nonsense-mediated mRNA decay, Molecular Cell (2022), https://doi.org/10.1016/j.molcel.2022.05.013

- Virus production, cell infection, and FACS sorting for the haploid genetic screen
- Flow cytometry for the haploid genetic screen
- Linear-amplification-mediated (LAM)-PCR and sequencing for the haploid genetic screen
- Steady-state NMD reporter assays of candidate NMD effectors identified in the haploid genetic screen
- NMD reporter mRNA half-life assay of candidate NMD effectors identified in the haploid genetic screen
- HEK293T cells and cell culture after verification of effectors identified in the haploid genetic screen, including mRNA half-life studies
- Generation and use of *FMR1*-KO iPSC line
- siRNA sequences
- Western blotting
- Immunoprecipitations
- RNA purification and RT-qPCR
- Mapping UPF1 phosphorylation sites using mass spectrometry
- Purification of UPF1 variants from *E. coli*
- *In vitro* kinase, helicase, ATPase, and RNA-binding assays

- QUANTIFICATION AND STATISTICAL ANALYSIS

SUPPLEMENTAL INFORMATION

Supplemental information can be found online at https://doi.org/10.1016/j.molcel.2022.05.013.

ACKNOWLEDGMENTS

We thank Alex Hewko, Yalan Tang, and Kelsey Williams for technical assistance; Joppe Nieuwenhuis, Thijn Brummelkamp, Sutapa Chakrabarti, Gail V.W. Johnson, Jeanne Stuckey, and Fabrice Lejeune for reagents and helpful advice; and Xavier Rambout and Tatsuaki Kurosaki for comments on the manuscript. The screen and some results were first published as Popp, M.W. and Maquat, L.E. A haploid genetic screening method for proteins influencing mammalian nonsense-mediated mRNA decay activity. bioRxiv 452490; https://doi.org/10.1101/452490. We thank the University of Rochester Medical Center (URMC) Flow Cytometry Core for help with flow cytometry, the URMC Mass Spectrometry Resource Laboratory for analyses (supported by NIH S10OD025242), and the University of Michigan Center for Structural Biology for purifying UPF1 variants from *E. coli*. This work was supported by NIH R01 GM059614 to L.E.M.; NIH R21NS104878 to C.P.; NIH U19MH107367 and NIH HG004659 to G.W.Y.; and a UR Provost's Award to L.E.M. and C.P. E.T.A. was supported in part by NIH T90 GR502287. S10 OD021489-01A1 supported the purchase of the Typhoon RGB Phosphorimager.

AUTHOR CONTRIBUTIONS

This project was initially conceived by M.W.P., who performed all aspects of the haploid-cell screen, including generating the required reagents. Subsequently H.C. and E.T.A. performed all experiments once they, together with L.E.M., decided to focus on AKT signaling; J.L.S. and G.W.Y. generated the *FMR1*-KO iPSCs from CVB iPSCs; and C.P. differentiated the iPSCs to NSCs and harvested the NSCs after culturing with or without Afu. E.T.A., H.C., and M.W.P. generated all figures. L.E.M., E.T.A., and M.W.P. wrote the manuscript with input from H.C., C.P., and J.L.S.

DECLARATION OF INTERESTS

G.W.Y. is a cofounder, member of the board of directors, on the scientific advisory board, an equity holder, and a paid consultant for Locanabio and Eclipse BioInnovations. G.W.Y. is a visiting professor at the National University of Singapore, and his interests have been reviewed and approved by the University of California, San Diego, in accordance with its conflict-of-interest policies.

Received: February 10, 2022
Revised: April 21, 2022
Accepted: May 10, 2022
Published: June 7, 2022

REFERENCES

Alexandrov, A., Shu, M.D., and Steitz, J.A. (2017). Fluorescence amplification method for forward genetic discovery of factors in human mRNA degradation. Mol. Cell *65*, 191–201.

Altomare, D.A., and Testa, J.R. (2005). Perturbations of the AKT signaling pathway in human cancer. Oncogene *24*, 7455–7464.

Anastasaki, C., Longman, D., Capper, A., Patton, E.E., and Cáceres, J.F. (2011). DHX34 and NBAS function in the NMD pathway and are required for embryonic development in zebrafish. Nucleic Acids Res. *39*, 3686–3694.

Augustyniak, J., Lenart, J., Lipka, G., Stepien, P.P., and Buzanska, L. (2019). Reference gene validation via RT-qPCR for human iPSC-derived neural stem cells and neural progenitors. Mol. Neurobiol. *56*, 6820–6832.

Baird, T.D., Cheng, K.C., Chen, Y.C., Buehler, E., Martin, S.E., Inglese, J., and Hogg, J.R. (2018). ICE1 promotes the link between splicing and nonsense-mediated mRNA decay. eLife *7*, e33178.

Bhattacharya, A., Czaplinski, K., Trifillis, P., He, F., Jacobson, A., and Peltz, S.W. (2000). Characterization of the biochemical properties of the human UPF1 gene product that is involved in nonsense-mediated mRNA decay. RNA *6*, 1226–1235.

Blomen, V.A., Májek, P., Jae, L.T., Bigenzahn, J.W., Nieuwenhuis, J., Staring, J., Sacco, R., van Diemen, F.R., Olk, N., Stukalov, A., et al. (2015). Gene essentiality and synthetic lethality in haploid human cells. Science *350*, 1092–1096.

Boehm, V., Kueckelmann, S., Gerbracht, J.V., Kallabis, S., Britto-Borges, T., Altmüller, J., Krüger, M., Dieterich, C., and Gehring, N.H. (2021). SMG5-SMG7 authorize nonsense-mediated mRNA decay by enabling SMG6 endonucleolytic activity. Nat. Commun. *12*, 3965.

Brockmann, M., Blomen, V.A., Nieuwenhuis, J., Stickel, E., Raaben, M., Bleijerveld, O.B., Altelaar, A.F.M., Jae, L.T., and Brummelkamp, T.R. (2017). Genetic wiring maps of single-cell protein states reveal an off-switch for GPCR signalling. Nature *546*, 307–311.

Brumbaugh, K.M., Otterness, D.M., Geisen, C., Oliveira, V., Brognard, J., Li, X., Lejeune, F., Tibbetts, R.S., Maquat, L.E., and Abraham, R.T. (2004). The mRNA surveillance protein hSMG-1 functions in genotoxic stress response pathways in mammalian cells. Mol. Cell *14*, 585–598.

Capela, A., and Temple, S. (2002). LeX/ssea-1 is expressed by adult mouse CNS stem cells, identifying them as nonependymal. Neuron *35*, 865–875.

Carette, J.E., Graat, H.C., Schagen, F.H., Abou El Hassan, M.A., Gerritsen, W.R., and van Beusechem, V.W. (2005). Replication-dependent transgene expression from a conditionally replicating adenovirus via alternative splicing to a heterologous splice-acceptor site. J. Gene Med. *7*, 1053–1062.

Carette, J.E., Guimaraes, C.P., Varadarajan, M., Park, A.S., Wuethrich, I., Godarova, A., Kotecki, M., Cochran, B.H., Spooner, E., Ploegh, H.L., and Brummelkamp, T.R. (2009). Haploid genetic screens in human cells identify host factors used by pathogens. Science *326*, 1231–1235.

Carette, J.E., Pruszak, J., Varadarajan, M., Blomen, V.A., Gokhale, S., Camargo, F.D., Wernig, M., Jaenisch, R., and Brummelkamp, T.R. (2010). Generation of iPSCs from cultured human malignant cells. Blood *115*, 4039–4042.

Carette, J.E., Guimaraes, C.P., Wuethrich, I., Blomen, V.A., Varadarajan, M., Sun, C., Bell, G., Yuan, B., Muellner, M.K., Nijman, S.M., et al. (2011a). Global gene disruption in human cells to assign genes to phenotypes by deep sequencing. Nat. Biotechnol. *29*, 542–546.

Carette, J.E., Pruszak, J., Varadarajan, M., Blomen, V.A., Gokhale, S., Camargo, F.D., Wernig, M., Jaenisch, R., and Brummelkamp, T.R. (2010).

Please cite this article in press as: Cho et al., AKT constitutes a signal-promoted alternative exon-junction complex that regulates nonsense-mediated mRNA decay, Molecular Cell (2022), https://doi.org/10.1016/j.molcel.2022.05.013

Generation of iPSCs from cultured human malignant cells. Blood *115*, 4039–4042.

Carette, J.E., Raaben, M., Wong, A.C., Herbert, A.S., Obernosterer, G., Mulherkar, N., Kuehne, A.I., Kranzusch, P.J., Griffin, A.M., Ruthel, G., et al. (2011b). Ebola virus entry requires the cholesterol transporter Niemann-Pick C1. Nature *477*, 340–343.

Chakrabarti, S., Jayachandran, U., Bonneau, F., Fiorini, F., Basquin, C., Domcke, S., Le Hir, H., and Conti, E. (2011). Molecular mechanisms for the RNA-dependent ATPase activity of UPF1 and its regulation by UPF2. Mol. Cell *41*, 693–703.

Chakrabarti, S., Bonneau, F., Schüssler, S., Eppinger, E., and Conti, E. (2014). Phospho-dependent and phospho-independent interactions of the helicase UPF1 with the NMD factors SMG5-SMG7 and SMG6. Nucleic Acids Res. *42*, 9447–9460.

Chambers, S.M., Fasano, C.A., Papapetrou, E.P., Tomishima, M., Sadelain, M., and Studer, L. (2009). Highly efficient neural conversion of human ES and iPS cells by dual inhibition of SMAD signaling. Nat. Biotechnol. *27*, 275–280.

Chamieh, H., Ballut, L., Bonneau, F., and Le Hir, H. (2008). NMD factors UPF2 and UPF3 bridge UPF1 to the exon junction complex and stimulate its RNA helicase activity. Nat. Struct. Mol. Biol. *15*, 85–93.

Cho, H., Kim, K.M., Han, S., Choe, J., Park, S.G., Choi, S.S., and Kim, Y.K. (2012). Staufen1-mediated mRNA decay functions in adipogenesis. Mol. Cell *46*, 495–506.

Cho, H., Rambout, X., Gleghorn, M.L., Nguyen, P.Q.T., Phipps, C.R., Miyoshi, K., Myers, J.R., Kataoka, N., Fasan, R., and Maquat, L.E. (2018). Transcriptional coactivator PGC-1alpha contains a novel CBP80-binding motif that orchestrates efficient target gene expression. Genes Dev *32*, 555–567.

Clerici, M., Mourão, A., Gutsche, I., Gehring, N.H., Hentze, M.W., Kulozik, A., Kadlec, J., Sattler, M., and Cusack, S. (2009). Unusual bipartite mode of interaction between the nonsense-mediated decay factors, UPF1 and UPF2. EMBO J. *28*, 2293–2306.

Cross, D.A., Alessi, D.R., Cohen, P., Andjelkovich, M., and Hemmings, B.A. (1995). Inhibition of glycogen synthase kinase-3 by insulin mediated by protein kinase B. Nature *378*, 785–789.

Dhara, S.K., Hasneen, K., Machacek, D.W., Boyd, N.L., Rao, R.R., and Stice, S.L. (2008). Human neural progenitor cells derived from embryonic stem cells in feeder-free cultures. Differentiation *76*, 454–464.

Dörpholz, G., Murgai, A., Jatzlau, J., Horbelt, D., Belverdi, M.P., Heroven, C., Schreiber, I., Wendel, G., Ruschke, K., Stricker, S., and Knaus, P. (2017). IRS4, a novel modulator of BMP/Smad and AKT signalling during early muscle differentiation. Sci. Rep. *7*, 8778.

Durand, S., Franks, T.M., and Lykke-Andersen, J. (2016). Hyperphosphorylation amplifies UPF1 activity to resolve stalls in nonsense-mediated mRNA decay. Nat. Commun. *7*, 12434.

Duronio, V. (2008). The life of a cell: apoptosis regulation by the PI3K/PKB pathway. Biochem. J. *415*, 333–344.

Ellis, P., Fagan, B.M., Magness, S.T., Hutton, S., Taranova, O., Hayashi, S., McMahon, A., Rao, M., and Pevny, L. (2004). SOX2, a persistent marker for multipotential neural stem cells derived from embryonic stem cells, the embryo or the adult. Dev. Neurosci. *26*, 148–165.

Eschenfeldt, W.H., Lucy, S., Millard, C.S., Joachimiak, A., and Mark, I.D. (2009). A family of LIC vectors for high-throughput cloning and purification of proteins. Methods Mol. Biol. *498*, 105–115.

Fiebiger, E., Hirsch, C., Vyas, J.M., Gordon, E., Ploegh, H.L., and Tortorella, D. (2004). Dissection of the dislocation pathway for type I membrane proteins with a new small molecule inhibitor, eeyarestatin. Mol. Biol. Cell *15*, 1635–1646.

Fiorini, F., Boudvillain, M., and Le Hir, H. (2013). Tight intramolecular regulation of the human UPF1 helicase by its N- and C-terminal domains. Nucleic Acids Res. *41*, 2404–2415.

Franks, T.M., Singh, G., and Lykke-Andersen, J. (2010). UPF1 ATPase-dependent mRNP disassembly is required for completion of nonsense- mediated mRNA decay. Cell *143*, 938–950.

Fritz, S.E., Ranganathan, S., Wang, C.D., and Hogg, J.R. (2020). The RNA-binding protein PTBP1 promotes ATPase-dependent dissociation of the RNA helicase UPF1 to protect transcripts from nonsense-mediated mRNA decay. J. Biol. Chem. *295*, 11613–11625.

Gardner, L.B. (2008). Hypoxic inhibition of nonsense-mediated RNA decay regulates gene expression and the integrated stress response. Mol. Cell. Biol. *28*, 3729–3741.

Gardner, L.B. (2010). Nonsense-mediated RNA decay regulation by cellular stress: implications for tumorigenesis. Mol. Cancer Res. *8*, 295–308.

Ge, Z., Quek, B.L., Beemon, K.L., and Hogg, J.R. (2016). Polypyrimidine tract binding protein 1 protects mRNAs from recognition by the nonsense-mediated mRNA decay pathway. eLife *5*, e11155.

Gehring, N.H., Kunz, J.B., Neu-Yilik, G., Breit, S., Viegas, M.H., Hentze, M.W., and Kulozik, A.E. (2005). Exon-junction complex components specify distinct routes of nonsense-mediated mRNA decay with differential cofactor requirements. Mol. Cell *20*, 65–75.

Gerbracht, J.V., Boehm, V., Britto-Borges, T., Kallabis, S., Wiederstein, J.L., Ciriello, S., Aschemeier, D.U., Krüger, M., Frese, C.K., Altmüller, J., et al. (2020). CASC3 promotes transcriptome-wide activation of nonsense-mediated decay by the exon junction complex. Nucleic Acids Res. *48*, 8626–8644.

Gong, C., Kim, Y.K., Woeller, C.F., Tang, Y., and Maquat, L.E. (2009). SMD and NMD are competitive pathways that contribute to myogenesis: effects on PAX3 and myogenin mRNAs. Genes Dev. *23*, 54–66.

Gowravaram, M., Bonneau, F., Kanaan, J., Maciej, V.D., Fiorini, F., Raj, S., Croquette, V., Le Hir, H., and Chakrabarti, S. (2018). A conserved structural element in the RNA helicase UPF1 regulates its catalytic activity in an isoform-specific manner. Nucleic Acids Res. *46*, 2648–2659.

Gross, C., and Bassell, G.J. (2012). Excess protein synthesis in FXS patient lymphoblastoid cells can be rescued with a p110beta-selective inhibitor. Mol. Med. *18*, 336–345.

Gross, C., Nakamoto, M., Yao, X., Chan, C.B., Yim, S.Y., Ye, K., Warren, S.T., and Bassell, G.J. (2010). Excess phosphoinositide 3-kinase subunit synthesis and activity as a novel therapeutic target in Fragile X syndrome. J. Neurosci. *30*, 10624–10638.

Gudikote, J.P., and Wilkinson, M.F. (2002). T-cell receptor sequences that elicit strong down-regulation of premature termination codon-bearing transcripts. EMBO J. *21*, 125–134.

Hosoda, N., Kim, Y.K., Lejeune, F., and Maquat, L.E. (2005). CBP80 promotes interaction of UPF1 with UPF2 during nonsense-mediated mRNA decay in mammalian cells. Nat. Struct. Mol. Biol. *12*, 893–901.

Hwang, J., Sato, H., Tang, Y., Matsuda, D., and Maquat, L.E. (2010). UPF1 association with the cap-binding protein, CBP80, promotes nonsense-mediated mRNA decay at two distinct steps. Mol. Cell *39*, 396–409.

Ishigaki, Y., Li, X., Serin, G., and Maquat, L.E. (2001). Evidence for a pioneer round of mRNA translation: mRNAs subject to nonsense-mediated decay in mammalian cells are bound by CBP80 and CBP20. Cell *106*, 607–617.

Isken, O., Kim, Y.K., Hosoda, N., Mayeur, G.L., Hershey, J.W., and Maquat, L.E. (2008). UPF1 phosphorylation triggers translational repression during nonsense-mediated mRNA decay. Cell *133*, 314–327.

Jacquemont, S., Pacini, L., Jønch, A.E., Cencelli, G., Rozenberg, I., He, Y., D'Andrea, L., Pedini, G., Eldeeb, M., Willemsen, R., et al. (2018). Protein synthesis levels are increased in a subset of individuals with Fragile X syndrome. Hum. Mol. Genet. *27*, 2039–2051.

Jae, L.T., Raaben, M., Riemersma, M., van Beusekom, E., Blomen, V.A., Velds, A., Kerkhoven, R.M., Carette, J.E., Topaloglu, H., Meinecke, P., et al. (2013). Deciphering the glycosylome of dystroglycanopathies using haploid screens for lassa virus entry. Science *340*, 479–483.

Jansen, V.M., Mayer, I.A., and Arteaga, C.L. (2016). Is there a future for AKT inhibitors in the treatment of cancer? Clin. Cancer Res. *22*, 2599–2601.

Please cite this article in press as: Cho et al., AKT constitutes a signal-promoted alternative exon-junction complex that regulates nonsense-mediated mRNA decay, Molecular Cell (2022), https://doi.org/10.1016/j.molcel.2022.05.013

Jia, J., Furlan, A., Gonzalez-Hilarion, S., Leroy, C., Gruenert, D.C., Tulasne, D., and Lejeune, F. (2015). Caspases shutdown nonsense-mediated mRNA decay during apoptosis. Cell Death Differ. *22*, 1754–1763.

Jia, K., Cui, C., Gao, Y., Zhou, Y., and Cui, Q. (2018). An analysis of aging-related genes derived from the Genotype-Tissue Expression project (GTEx). Cell Death Discov. *4*, 26.

Kang, Y., Zhou, Y., Li, Y., Han, Y., Xu, J., Niu, W., Li, Z., Liu, S., Feng, H., Huang, W., et al. (2021). A human forebrain organoid model of Fragile X syndrome exhibits altered neurogenesis and highlights new treatment strategies. Nat. Neurosci. *24*, 1377–1391.

Karam, R., Wengrod, J., Gardner, L.B., and Wilkinson, M.F. (2013). Regulation of nonsense-mediated mRNA decay: implications for physiology and disease. Biochim. Biophys. Acta *1829*, 624–633.

Karam, R., Lou, C.H., Kroeger, H., Huang, L., Lin, J.H., and Wilkinson, M.F. (2015). The unfolded protein response is shaped by the NMD pathway. EMBO Rep. *16*, 599–609.

Kashima, I., Yamashita, A., Izumi, N., Kataoka, N., Morishita, R., Hoshino, S., Ohno, M., Dreyfuss, G., and Ohno, S. (2006). Binding of a novel SMG-1-UPF1-eRF1-eRF3 complex (SURF) to the exon junction complex triggers UPF1 phosphorylation and nonsense-mediated mRNA decay. Genes Dev. *20*, 355–367.

Kim, Y.K., Furic, L., Desgroseillers, L., and Maquat, L.E. (2005). Mammalian Staufen1 recruits Upf1 to specific mRNA 3'UTRs so as to elicit mRNA decay. Cell *120*, 195–208.

Kim, Y.K., and Maquat, L.E. (2019). UPFront and center in RNA decay: UPF1 in nonsense-mediated mRNA decay and beyond. RNA *25*, 407–422.

Kishor, A., Fritz, S.E., and Hogg, J.R. (2019). Nonsense-mediated mRNA decay: the challenge of telling right from wrong in a complex transcriptome. Wiley Interdiscip. Rev. RNA *10*, e1548.

Kurosaki, T., and Maquat, L.E. (2013). Rules that govern UPF1 binding to mRNA 3′ UTRs. Proceedings of the National Academy of Sciences of the United States of America. *110*, 3357–3362. https://doi.org/10.1073/pnas.1219908110.

Kurosaki, T., Li, W., Hoque, M., Popp, M.W., Ermolenko, D.N., Tian, B., and Maquat, L.E. (2014). A post-translational regulatory switch on UPF1 controls targeted mRNA degradation. Genes Dev. *28*, 1900–1916.

Kurosaki, T., Popp, M.W., and Maquat, L.E. (2019). Quality and quantity control of gene expression by nonsense-mediated mRNA decay. Nat. Rev. Mol. Cell Biol. *20*, 406–420.

Kurosaki, T., Imamachi, N., Pröschel, C., Mitsutomi, S., Nagao, R., Akimitsu, N., and Maquat, L.E. (2021a). Loss of the Fragile X syndrome protein FMRP results in misregulation of nonsense-mediated mRNA decay. Nat. Cell Biol. *23*, 40–48.

Kurosaki, T., Sakano, H., Pröschel, C., Wheeler, J., Hewko, A., and Maquat, L.E. (2021b). NMD abnormalities during brain development in the *Fmr1*-knockout mouse model of Fragile X syndrome. Genome Biol. *22*, 317.

Lee, S.R., Pratt, G.A., Martinez, F.J., Yeo, G.W., and Lykke-Andersen, J. (2015). Target discrimination in nonsense-mediated mRNA decay requires UPF1 ATPase activity. Mol. Cell *59*, 413–425.

Li, T., Shi, Y., Wang, P., Guachalla, L.M., Sun, B., Joerss, T., Chen, Y.S., Groth, M., Krueger, A., Platzer, M., et al. (2015). SMG6/EST1 licenses embryonic stem cell differentiation via nonsense-mediated mRNA decay. EMBO J. *34*, 1630–1647.

Lin, K., Lin, J., Wu, W.I., Ballard, J., Lee, B.B., Gloor, S.L., Vigers, G.P., Morales, T.H., Friedman, L.S., Skelton, N., and Brandhuber, B.J. (2012). An ATP-site on-off switch that restricts phosphatase accessibility of AKT. Sci. Signal. *5*, ra37.

Livak, K.J., and Schmittgen, T.D. (2001). Analysis of relative gene expression data using real-time quantitative PCR and the $2(-\Delta\Delta C_T)$ method. Methods *25*, 402–408.

Loh, B., Jonas, S., and Izaurralde, E. (2013). The SMG5-SMG7 heterodimer directly recruits the CCR4-NOT deadenylase complex to mRNAs containing nonsense codons via interaction with POP2. Genes Dev. *27*, 2125–2138.

Longman, D., Hug, N., Keith, M., Anastasaki, C., Patton, E.E., Grimes, G., and Cáceres, J.F. (2013). DHX34 and NBAS form part of an autoregulatory NMD circuit that regulates endogenous RNA targets in human cells, zebrafish and *Caenorhabditis elegans*. Nucleic Acids Res. *41*, 8319–8331.

Longman, D., Jackson-Jones, K.A., Maslon, M.M., Murphy, L.C., Young, R.S., Stoddart, J.J., Hug, N., Taylor, M.S., Papadopoulos, D.K., and Cáceres, J.F. (2020). Identification of a localized nonsense-mediated decay pathway at the endoplasmic reticulum. Genes Dev. *34*, 1075–1088.

Lou, C.H., Dumdie, J., Goetz, A., Shum, E.Y., Brafman, D., Liao, X., Mora-Castilla, S., Ramaiah, M., Cook-Andersen, H., Laurent, L., and Wilkinson, M.F. (2016). Nonsense-mediated RNA decay influences human embryonic stem cell fate. Stem Cell Rep. *6*, 844–857.

Mabin, J.W., Woodward, L.A., Patton, R.D., Yi, Z., Jia, M., Wysocki, V.H., Bundschuh, R., and Singh, G. (2018). The exon junction complex undergoes a compositional switch that alters mRNP structure and nonsense-mediated mRNA decay activity. Cell Rep. *25*, 2431–2446.e7.

Malecki, C., Hambly, B.D., Jeremy, R.W., and Robertson, E.N. (2020). The RNA-binding Fragile-X mental retardation protein and its role beyond the brain. Biophys. Rev. *12*, 903–916.

Manning, B.D., and Cantley, L.C. (2007). AKT/PKB signaling: navigating downstream. Cell *129*, 1261–1274.

Manning, B.D., and Toker, A. (2017). AKT/PKB signaling: navigating the network. Cell *169*, 381–405.

Matsuoka, S., Ballif, B.A., Smogorzewska, A., McDonald, E.R., 3rd, Hurov, K.E., Luo, J., Bakalarski, C.E., Zhao, Z., Solimini, N., Lerenthal, Y., et al. (2007). ATM and ATR substrate analysis reveals extensive protein networks responsive to DNA damage. Science *316*, 1160–1166.

McIlwain, D.R., Pan, Q., Reilly, P.T., Elia, A.J., McCracken, S., Wakeham, A.C., Itie-Youten, A., Blencowe, B.J., and Mak, T.W. (2010). SMG1 is required for embryogenesis and regulates diverse genes via alternative splicing coupled to nonsense-mediated mRNA decay. Proc. Natl. Acad. Sci. USA *107*, 12186–12191.

Medghalchi, S.M., Frischmeyer, P.A., Mendell, J.T., Kelly, A.G., Lawler, A.M., and Dietz, H.C. (2001). RENT1, a trans-effector of nonsense-mediated mRNA decay, is essential for mammalian embryonic viability. Hum. Mol. Genet. *10*, 99–105.

Mertins, P., Yang, F., Liu, T., Mani, D.R., Petyuk, V.A., Gillette, M.A., Clauser, K.R., Qiao, J.W., Gritsenko, M.A., Moore, R.J., et al. (2014). Ischemia in tumors induces early and sustained phosphorylation changes in stress kinase pathways but does not affect global protein levels. Mol. Cell. Proteomics *13*, 1690–1704.

Mookherjee, P., Quintanilla, R., Roh, M.S., Zmijewska, A.A., Jope, R.S., and Johnson, G.V. (2007). Mitochondrial-targeted active Akt protects SH-SY5Y neuroblastoma cells from staurosporine-induced apoptotic cell death. J Cell Biochem *102*, 196–210.

Moschella, P.C., McKillop, J., Pleasant, D.L., Harston, R.K., Balasubramanian, S., and Kuppuswamy, D. (2013). mTOR complex 2 mediates AKT phosphorylation that requires PKCε in adult cardiac muscle cells. Cell. Signal. *25*, 1904–1912.

Nagy, E., and Maquat, L.E. (1998). A rule for termination-codon position within intron-containing genes: when nonsense affects RNA abundance. Trends Biochem. Sci. *23*, 198–199.

Nasif, S., Contu, L., and Mühlemann, O. (2018). Beyond quality control: the role of nonsense-mediated mRNA decay (NMD) in regulating gene expression. Semin. Cell Dev. Biol. *75*, 78–87.

Nickless, A., Jackson, E., Marasa, J., Nugent, P., Mercer, R.W., Piwnica-Worms, D., and You, Z. (2014). Intracellular calcium regulates nonsense-mediated mRNA decay. Nat. Med. *20*, 961–966.

Nieuwenhuis, J., Adamopoulos, A., Bleijerveld, O.B., Mazouzi, A., Stickel, E., Celie, P., Altelaar, M., Knipscheer, P., Perrakis, A., Blomen, V.A., and Brummelkamp, T.R. (2017). Vasohibins encode tubulin detyrosinating activity. Science *358*, 1453–1456.

Please cite this article in press as: Cho et al., AKT constitutes a signal-promoted alternative exon-junction complex that regulates nonsense-mediated mRNA decay, Molecular Cell (2022), https://doi.org/10.1016/j.molcel.2022.05.013

Nitulescu, G.M., Margina, D., Juzenas, P., Peng, Q., Olaru, O.T., Saloustros, E., Fenga, C., Spandidos, D.A., Libra, M., and Tsatsakis, A.M. (2016). AKT inhibitors in cancer treatment: the long journey from drug discovery to clinical use (Review). Int. J. Oncol. *48*, 869–885.

Ohnishi, T., Yamashita, A., Kashima, I., Schell, T., Anders, K.R., Grimson, A., Hachiya, T., Hentze, M.W., Anderson, P., and Ohno, S. (2003). Phosphorylation of hUPF1 induces formation of mRNA surveillance complexes containing hSMG-5 and hSMG-7. Mol. Cell *12*, 1187–1200.

Paillusson, A., Hirschi, N., Vallan, C., Azzalin, C.M., and Mühlemann, O. (2005). A GFP-based reporter system to monitor nonsense-mediated mRNA decay. Nucleic Acids Res. *33*, e54.

Palma, M., Leroy, C., Salomé-Desnoulez, S., Werkmeister, E., Kong, R., Mongy, M., Le Hir, H., and Lejeune, F. (2021). A role for AKT1 in nonsense-mediated mRNA decay. Nucleic Acids Res. *49*, 11022–11037.

Park, E., Gleghorn, M.L., and Maquat, L.E. (2013). Staufen2 functions in Staufen1-mediated mRNA decay by binding to itself and its paralog and promoting UPF1 helicase but not ATPase activity. Proc. Natl. Acad. Sci. USA *110*, 405–412.

Park, J., Ahn, S., Jayabalan, A.K., Ohn, T., Koh, H.C., and Hwang, J. (2016). Insulin signaling augments eIF4E-dependent nonsense-mediated mRNA decay in mammalian cells. Biochim. Biophys. Acta *1859*, 896–905.

Pellerin, D., Çaku, A., Fradet, M., Bouvier, P., Dubé, J., and Corbin, F. (2016). Lovastatin corrects ERK pathway hyperactivation in Fragile X syndrome: potential of platelet's signaling cascades as new outcome measures in clinical trials. Biomarkers *21*, 497–508.

Popp, M.W., and Maquat, L.E. (2015). Attenuation of nonsense-mediated mRNA decay facilitates the response to chemotherapeutics. Nat. Commun. *6*, 6632.

Popp, M.W., and Maquat, L.E. (2018). Nonsense-mediated mRNA decay and cancer. Curr. Opin. Genet. Dev. *48*, 44–50.

Pruszak, J., Ludwig, W., Blak, A., Alavian, K., and Isacson, O. (2009). CD15, CD24, and CD29 define a surface biomarker code for neural lineage differentiation of stem cells. Stem Cells *27*, 2928–2940.

Qi, Y., Zhang, X.J., Renier, N., Wu, Z., Atkin, T., Sun, Z., Ozair, M.Z., Tchieu, J., Zimmer, B., Fattahi, F., et al. (2017). Combined small-molecule inhibition accelerates the derivation of functional cortical neurons from human pluripotent stem cells. Nat. Biotechnol. *35*, 154–163.

Razak, K.A., Dominick, K.C., and Erickson, C.A. (2020). Developmental studies in Fragile X syndrome. J. Neurodev. Disord. *12*, 13.

Reubinoff, B.E., Itsykson, P., Turetsky, T., Pera, M.F., Reinhartz, E., Itzik, A., and Ben-Hur, T. (2001). Neural progenitors from human embryonic stem cells. Nat. Biotechnol. *19*, 1134–1140.

Ruggero, D., and Sonenberg, N. (2005). The Akt of translational control. Oncogene *24*, 7426–7434.

Schlautmann, L.P., and Gehring, N.H. (2020). A day in the life of the exon junction complex. Biomolecules *10*, 866.

Staring, J., von Castelmur, E., Blomen, V.A., van den Hengel, L.G., Brockmann, M., Baggen, J., Thibaut, H.J., Nieuwenhuis, J., Janssen, H., van Kuppeveld, F.J., et al. (2017). PLA2G16 represents a switch between entry and clearance of Picornaviridae. Nature *541*, 412–416.

Stewart, S.A., Dykxhoorn, D.M., Palliser, D., Mizuno, H., Yu, E.Y., An, D.S., Sabatini, D.M., Chen, I.S., Hahn, W.C., Sharp, P.A., Weinberg, R.A., and Novina, C.D. (2003). Lentivirus-delivered stable gene silencing by RNAi in primary cells. RNA *9*, 493–501.

Suardi, G.A.M., and Haddad, L.A. (2020). FMRP ribonucleoprotein complexes and RNA homeostasis. Adv. Genet. *105*, 95–136.

Ulm, J.W., Perron, M., Sodroski, J., and Mulligan, R.C. (2007). Complex determinants within the Moloney murine leukemia virus capsid modulate susceptibility of the virus to Fv1 and Ref1-mediated restriction. Virology *363*, 245–255.

Vivanco, I., Chen, Z.C., Tanos, B., Oldrini, B., Hsieh, W.Y., Yannuzzi, N., Campos, C., and Mellinghoff, I.K. (2014). A kinase-independent function of AKT promotes cancer cell survival. eLife *3*.

Wang, D., Zavadil, J., Martin, L., Parisi, F., Friedman, E., Levy, D., Harding, H., Ron, D., and Gardner, L.B. (2011). Inhibition of nonsense-mediated RNA decay by the tumor microenvironment promotes tumorigenesis. Mol. Cell. Biol. *31*, 3670–3680.

Weischenfeldt, J., Damgaard, I., Bryder, D., Theilgaard-Mönch, K., Thoren, L.A., Nielsen, F.C., Jacobsen, S.E., Nerlov, C., and Porse, B.T. (2008). NMD is essential for hematopoietic stem and progenitor cells and for eliminating by-products of programmed DNA rearrangements. Genes Dev. *22*, 1381–1396.

Wilson, K.F., Wu, W.J., and Cerione, R.A. (2000). Cdc42 stimulates RNA splicing via the S6 kinase and a novel S6 kinase target, the nuclear cap-binding complex. J. Biol. Chem. *275*, 37307–37310.

Yamaji, M., Ota, A., Wahiduzzaman, M., Karnan, S., Hyodo, T., Konishi, H., Tsuzuki, S., Hosokawa, Y., and Haniuda, M. (2017). Novel ATP-competitive AKT inhibitor afuresertib suppresses the proliferation of malignant pleural mesothelioma cells. Cancer Med. *6*, 2646–2659.

Yamashita, A., Izumi, N., Kashima, I., Ohnishi, T., Saari, B., Katsuhata, Y., Muramatsu, R., Morita, T., Iwamatsu, A., Hachiya, T., et al. (2009). SMG-8 and SMG-9, two novel subunits of the SMG-1 complex, regulate remodeling of the mRNA surveillance complex during nonsense-mediated mRNA decay. Genes Dev. *23*, 1091–1105.

Yamashita, A., Ohnishi, T., Kashima, I., Taya, Y., and Ohno, S. (2001). Human SMG-1, a novel phosphatidylinositol 3-kinase-related protein kinase, associates with components of the mRNA surveillance complex and is involved in the regulation of nonsense-mediated mRNA decay. Genes Dev *15*, 2215–2228.

Yi, Z., Sanjeev, M., and Singh, G. (2021). The branched nature of the nonsense-mediated mRNA decay pathway. Trends Genet. *37*, 143–159.

Zhu, X., Zhang, H., and Mendell, J.T. (2020). Ribosome recycling by ABCE1 links lysosomal function and iron homeostasis to 3′ UTR-directed regulation and nonsense-mediated decay. Cell Rep. *32*, 107895.

Please cite this article in press as: Cho et al., AKT constitutes a signal-promoted alternative exon-junction complex that regulates nonsense-mediated mRNA decay, Molecular Cell (2022), https://doi.org/10.1016/j.molcel.2022.05.013

STAR★METHODS

KEY RESOURCES TABLE

REAGENT or RESOURCE	SOURCE	IDENTIFIER
Antibodies		
α-FLAG (1:1000)	Sigma	A8592
α-HA (1:1000)	Roche	12013819001
α-Vimentin (1:1000)	Abcam	ab8978
α-UPF1 (1:1000)	Kim et al. (2005)	Cell. 2005 Jan; 120(2):195-208
α-UPF1(S1116) (1: 1000)	Sigma	07-1016
α-UPF2 (1: 500)	Santa Cruz, Cho et al. (2012)	sc-20227, Mol Cell. 2012 May 25;46(4):495-506
α-UPF3X (1: 1000)	Abcam	ab134566
α-eIF4A3 (1: 1000)	Bethyl	A302-980A, A302-981A
α-CBP80 (1: 1000)	Cho et al. (2018)	Genes Dev. 2018 Apr; 32(7-8):555-567
α-eIF4E (1: 1000)	Bethyl	A301-153A
α-RNPS1 (1: 1000)	Proteintech	10555-1-AP
α-CASC3 (1: 1000)	Santa Cruz	sc-376186
α-RBM8A (1: 1000)	Sigma	Y1253
α-MAGOH (1: 1000)	Santa Cruz	sc-56724
α-PABPC1 (1: 1000)	Abcam	ab21060
α-GAPDH (1: 1000)	Cell Signaling	#2118
α-Tubulin (1: 1000)	Cell Signaling	#3873
α-Calnexin (1: 1000)	Enzo	ADI-SPA-865
α-SMG1 (1: 1000)	Cell Signaling	#9149
α-pan-AKT (1: 1000)	Cell Signaling	#4691, #2920
α-p-pan AKT (T308) (1: 1000)	Cell Signaling	#5106
α-p-pan AKT (S473) (1: 1000)	Cell Signaling	#4060, #4051
α-AKT1 (1: 1000)	Cell Signaling	#2938
α-AKT2 (1: 1000)	Cell Signaling	#2964
α-AKT3 (1: 1000)	Cell Signaling	#3788
α-ROBO1 (1: 1000)	Proteintech	20219-1-AP
α-ROBO2 (1: 1000)	Cell Signaling	#45568
α-SLIT2 (1: 1000)	Cell Signaling	#47600
α-MYO10 (1: 1000)	Sigma	HPA024223
α-PTPRD (1: 1000)	Abcam	ab233806
α-IL1RAPL1 (1: 1000)	Proteintech	21609-1-AP
α-Phospho-Akt Substrate (RXXpS/pT) (1: 1000)	Cell Signaling	#9614
α-p-mTOR(S2446) (1: 1000)	Cell Signaling	#2971
α-GSK3β (S9) (1: 1000)	Cell Signaling	#12456
α-p-GSK3β (S9) (1: 1000)	Cell Signaling	#5558
α-SMG5 (1: 1000)	Abcam	ab129107
α-SMG6 (1: 1000)	Abcam	ab87539
α-SMG7 (1: 1000)	Bethyl	A302-170A
α-FMRP (1: 1000)	Abcam	ab17722
α-SOX1 (1: 100)	R&D Systems	AF3369
α-SOX2 (1: 50)	Calbiochem	SC1002

(*Continued on next page*)

Please cite this article in press as: Cho et al., AKT constitutes a signal-promoted alternative exon-junction complex that regulates nonsense-mediated mRNA decay, Molecular Cell (2022), https://doi.org/10.1016/j.molcel.2022.05.013

Continued

REAGENT or RESOURCE	SOURCE	IDENTIFIER
α-Vimentin (1: 100)	Cell Signaling	5741
α-Nestin (1: 100)	Abcam	ab105389
α-PAX6 (1: 100)	Abcam	ab78545
IgG from rabbit serum	Sigma-Aldrich	I5006
Peroxidase IgG Fraction Monoclonal Mouse Anti-Rabbit IgG, light chain specific	Jackson ImmunoResearch	211-032-171
Goat anti-Rabbit IgG (H+L) Cross-Adsorbed Secondary Antibody, HRP	Invitrogen	31462
Goat anti-Mouse IgG (H+L) Poly-HRP Secondary Antibody, HRP	Invitrogen	32230
Anti-Goat IgG (whole molecule)–Peroxidase antibody produced in rabbit	Sigma	A5420
Donkey anti-Goat IgG, Alexa 546 (2 μg/mL)	Thermo Fisher Scientific	A11056
Goat anti-Mouse IgG, Alexa 488 (2 μg/mL)	Thermo Fisher Scientific	A32723
Goat anti-Mouse IgG, Alexa 568 (2 μg/mL)	Thermo Fisher Scientific	A11004
Goat anti-Rabbit IgG, Alexa 568 (2 μg/mL)	Thermo Fisher Scientific	A11011
Goat anti-Rabbit IgG, Alexa 488 (2 μg/mL)	Thermo Fisher Scientific	A32721
Bacterial and virus strains		
One Shot™ MAX Efficiency™ DH5α-T1R Competent Cells	Invitrogen	12297016
Rosetta 2 ™ BL21 (DE3) Competent Cells	Novagen	71402
Ad5CMV-Cre virus	University of Iowa Gene Transfer Vector Core	N/A
Chemicals, peptides, and recombinant proteins		
DMEM, high glucose, pyruvate	Gibco	1195065
Iscove's Modified Dulbecco's Medium (IMDM)	Gibco	12440053
StemFlex Medium	Gibco	A3349401
Essential 6™ Medium	Gibco	A1516401
DMEM/F12 Medium	Gibco	11320033
Avantor Seradigm Premium Grade Fetal Bovine Serum (FBS)	VWR	97068-085
Goat Serum	EMD Millipore	S26-100ML
GlutaMAX (100x)	Gibco	35050061
N-2 Supplement (100x)	Gibco	17502048
B-27™ Supplement (50X)	Gibco	17504044
Matrigel	Corning Life Sciences	354230
Penicillin-Streptomycin (10,000 U/mL)	Gibco	15140122
Trypsin-EDTA (0.25%), phenol red	Gibco	25200056
ACCUTASE™ Cell detachment solution	Stem Cell Technologies	07920
Turbofectin 8.0	Origene	TF81001
Lipofectamine™ 2000	Invitrogen	11668019
Lipofectamine™ RNAiMAX	Invitrogen	13778075
Opti-MEM™ I Reduced Serum Medium	Gibco	31985070
HBSS (10X), calcium, magnesium, no phenol red	Glibco	14065056
PBS, pH 7.4	Gibco	10010023
Halt™ Protease and Phosphatase Inhibitor Cocktail	Thermo Scientific	78442
Protein A-Agarose	Roche	10037256

(*Continued on next page*)

Please cite this article in press as: Cho et al., AKT constitutes a signal-promoted alternative exon-junction complex that regulates nonsense-mediated mRNA decay, Molecular Cell (2022), https://doi.org/10.1016/j.molcel.2022.05.013

Continued

REAGENT or RESOURCE	SOURCE	IDENTIFIER
Pierce™ Anti-c-Myc-Magnetic Beads	Thermo	88842
ANTI-FLAG® M2 Affinity Gel	Sigma	A2220
TRIzol™ Reagent	Invitrogen	15596018
RQ1 RNase-free DNase	Promega	M6101
RNase OUT™ Recombinant Ribonuclease Inhibitor	Invitrogen	10777019
cOmplete™ Protease Inhibitor Cocktail	Roche	11697498001
SuperScript™ III Reverse Transcriptase	Invitrogen	18080044
Random Primers	Invitrogen	58875
Fast SYBR Green Master Mix	Applied Biosystems	4385614
PerfeCTa SYBR Green SuperMix, Low ROX™	Quantabio	95056-02K
Acrylamide/bis-acrylamide 29:1 (40%)	Fisher Scientific	BP1408-1
Ammonium persulfate, crystal	Mallinckrodt Chemicals	3460-04
UltraPure TEMED	Thermo Fisher Scientific, Invitrogen	15524010
Sodium dodecyl sulfate	Sigma-Aldrich	75746-1KG
TWEEN 20	Sigma-Aldrich	P7949-500ML
Bovine Serum Albumin (BSA)	Rockland Immunochemicals	BSA-50
MEGAscript™ T7 Transcription Kit	Invitrogen	AM1334
Lenti-X™ Packaging Single Shots	Clontech	631275
QIAamp DNA Mini Kit	Qiagen	51304
QIAquick PCR Purification Kit	Qiagen	28104
RNA Clean and Concentrator Kit	Zymo Research	R1017
ZR small-RNA PAGE Recovery Kit	Zymo Research	R1070
rATP	Promega	P1132
ATP, [γ-32P]	Perkin Elmer	NEG002A100UC
Phusion High-Fidelity DNA Polymerase	NEB	E0553S
AmpliTaq™ DNA Polymerase	Thermo Fisher Scientific	N8080160
ApaI	NEB	R0114S
KpnI-HF	NEB	R3142S
XhoI	NEB	R0146S
BsiWI	NEB	R0553L
SspI	NEB	R0132S
Quick CIP	NEB	M0525S
T4 DNA Ligase	Takara Bio	2011B
T4 DNA Polymerase, LIC-qualified	Novagen	70099
Circligase II	Lucigen	CL1021K
Zeocin™ Selection Reagent	Gibco	R25001
Trypsin, MS Grade	Promega	V5280
Pierce™ Chymotrypsin Protease (TLCK treated), MS Grade	Thermo Fisher Scientific	90056
Pierce™ Glu-C Protease, MS Grade	Thermo Fisher Scientific	90054
Protamine sulfate	MP Biomedicals	02194729-CF
Dynabeads™ M-270 Streptavidin	Thermo	65305
CD15 MicroBeads, human	Miltenyi Biotec	130-046-601
NE-PER™ Nuclear and Cytoplasmic Extraction Reagents	Thermo	78833
Gibco™ Insulin, human recombinant, zinc solution	Thermo	12585014

(*Continued on next page*)

Please cite this article in press as: Cho et al., AKT constitutes a signal-promoted alternative exon-junction complex that regulates nonsense-mediated mRNA decay, Molecular Cell (2022), https://doi.org/10.1016/j.molcel.2022.05.013

Continued

REAGENT or RESOURCE	SOURCE	IDENTIFIER
Dimethyl sulfoxide ≥99.9%, Ultra Pure Grade	VWR	97063-136
4% Paraformaldehyde	MP Biomedicals	MP021501465
Doxycycline	Sigma	D3072
Okadaic acid	LC Laboratories	O-5857
Y27632 ROK inhibitor	HelloBio	HB2297
SB431542 Smad inhibitor	Cayman Chemical	13031
LDN-193189 Smad inhibitor	Cayman Chemical	11802
XAV 939 Tankyrase inhibitor	Tocris	3748
Epidermal growth factor	PeproTech	500-P45
Fibroblast growth factor-2	Miltenyi Biotec	130-093-839
LDN-193189 ALK2/3 inhibitor	MedChem Express	HY-12071
CHIR-99021 GSK-3α/β inhibitor	MedChem Express	HY-10182
Afuresertib (GSK2110183)	Selleckchem	S7521
Critical commercial assays		
AKT1 Kinase Enzyme System	Promega	V1911
AKT2 Kinase Enzyme System	Promega	V3861
AKT3 Kinase Enzyme System	Promega	V4010
ADP-Glo™ Kinase Assay	Promega	V6930
Experimental models: Cell lines		
Lenti-X HEK293T cells	Clontech	632180
HEK293T cells	ATCC	CRL-3216™
HEK293 Tet-OFF Advanced cells	Clontech	631152
Isogenic NSCs	This paper	Yeo Lab
HAP1 cells	Carette et al. (2010)	Blood. 2010 May; 115(20):4039-42
Sf9 cells	CRL-1711	ATCC
Oligonucleotides		
CTL siRNA	Sigma	N/A
SilencerTM Negative Control No.1 siRNA	Ambion	N/A
UPF1 siRNA 5'-GAUGCAGUUCCGCUCCAUU-3'	Kurosaki et al. (2014)	Genes Dev. 2014 Sep; 28(17):1900-16
ROBO1 siRNA: 5'-GGACAUAAAUCUCAACUUG-3'	This paper	N/A
ROBO2 siRNA: 5'-GCAAAUAGUUAAAGAAGCA-3'	This paper	N/A
SLIT2 siRNA: 5'-AGAUAUACCUGGAGACAUU-3'	This paper	N/A
MYO10 siRNA: 5'-GGACAUAAAUCUCAACUUG-3'	This paper	N/A
PTPRD siRNA: 5'CUGGGAACACAAUUCCACCAU-3'	This paper	N/A
IL1RAPL1 siRNA	Horizon	J-007961-05-0002
AKT3 siRNA: 5'-GAAUGAAUUGUAGUCCAACU-3'	This paper	N/A
AKT1 siRNA: 5'GAAGGAAGUCAUCGUGGCCAA-3'	This paper	N/A
AKT2 siRNA: 5'-CUCUUCGAGCUCAUCCUCA-3'	This paper	N/A

(*Continued on next page*)

Please cite this article in press as: Cho et al., AKT constitutes a signal-promoted alternative exon-junction complex that regulates nonsense-mediated mRNA decay, Molecular Cell (2022), https://doi.org/10.1016/j.molcel.2022.05.013

Continued

REAGENT or RESOURCE	SOURCE	IDENTIFIER
AKT1, *AKT2/3* siRNAs: 5'-UGCCCUUCUACAACCAGGA-3', 5'-CUCUUCAGAUGCAAAAUCA-3'	Park et al. (2016)	Biochim Biophys Acta. 2016 Jul;1859(7):896-905.
SMG1 siRNA: 5'-CCAGGACACGAGGAAACUG-3'	Kurosaki et al. (2014)	Genes Dev. 2014 Sep; 28(17):1900-16
UPF2 siRNA: 5'-CUAGUGAGAUAAUUAGUCCAG-3'	Kurosaki et al. (2014)	Genes Dev. 2014 Sep; 28(17):1900-16
FMR1 sgRNA #1 5'-AATCGATTGGTGGTTGTCG -3'	This paper	N/A
FMR1 sgRNA #2 5'-CAACCACCAATCGATTTCA-3'	This paper	N/A
RT-qPCR primers: see Table S5	This paper	N/A
Cloning primers: see Table S6	This paper	N/A
Recombinant DNA		
pCG-GAG/Pol	Ulm et al. (2007)	N/A
pCMV-VSV-G	Stewart et al. (2003)	Addgene #8454
pAdvantage	Promega	E1711
pGT GFP(0)	Carette et al. (2011a)	Nat Biotechnol. 2011 Jun; 29(6):542-546
pGT GFP(+1)	Carette et al. (2011a)	Nat Biotechnol. 2011 Jun; 29(6):542-546
pGT GFP(+2)	Carette et al. (2011a)	Nat Biotechnol. 2011 Jun; 29(6):542-546
pmCherry-C1	Clontech	632524
+(JC Intron)	Popp and Maquat (2015)	Nat. Commun. 2015 Mar; 26(6):6632
Δ(JC Intron)	Popp and Maquat (2015)	Nat. Commun. 2015 Mar; 26(6):6632
3XFLAG-mCherry	Popp and Maquat (2015)	Nat. Commun. 2015 Mar; 26(6):6632
HA-Cerulean	Popp and Maquat (2015)	Nat. Commun. 2015 Mar; 26(6):6632
Tet OFF β-Globin Norm	Popp and Maquat (2015)	Nat. Commun. 2015 Mar; 26(6):6632
Tet OFF β-Globin Ter	Popp and Maquat (2015)	Nat. Commun. 2015 Mar; 26(6):6632
β-Globin Norm	Kurosaki and Maquat (2013)	PNAS. 2013 Feb;110(9):3357-62
β-Globin Ter	Kurosaki and Maquat (2013)	PNAS. 2013 Feb;110(9):3357-62
3X-FLAG-β-Globin Norm	Kurosaki et al. (2021a)	Nature Cell Biology. 2021 Jan; (23):40-48
3X-FLAG-β-Globin Ter	Kurosaki et al. (2021a)	Nature Cell Biology. 2021 Jan; (23):40-48
MUP	Kim et al. (2005)	Cell. 2005 Jan; 120(2):195-208
YFP-GPx1 Norm	Palma et al. (2021)	NAR. 2021 Oct; 49(19) 11022-37
YFP-GPx1 Ter	Palma et al. (2021)	NAR. 2021 Oct; 49(19) 11022-37
pCMV-Myc	Clontech	635689
pCMV-Myc-UPF1^{R}(WT)	Isken et al. (2008)	Cell. 2008 Apr; 133(2):314-27
pCMV-Myc-UPF1^{R}(T151D)	This paper	N/A
pCMV-Myc-UPF1^{R}(T151A)	This paper	N/A
pMCFG7-6xHis-TEV-UPF1(115-914) WT	This paper	N/A
pMCFG7-6xHis-TEV-UPF1(115-914) T151D	This paper	N/A
pMCFG7-6xHis-TEV-UPF1(115-914) T151A	This paper	N/A
Software and algorithms		
HAP1 screen analysis	Carette et al. (2010)	https://github.com/BrummelkampResearch
Image J	NIH	https://imagej.nih.gov/ij/
Lecia LAS AF	Lecia	N/A
Other		
LSR-II flow cytometer	BD Biosciences	N/A
HiSeq2500	Illumina	SY–401–2501

(*Continued on next page*)

Please cite this article in press as: Cho et al., AKT constitutes a signal-promoted alternative exon-junction complex that regulates nonsense-mediated mRNA decay, Molecular Cell (2022), https://doi.org/10.1016/j.molcel.2022.05.013

Continued

REAGENT or RESOURCE	SOURCE	IDENTIFIER
Ni-NTA Superflow Cartridges	Qiagen	30761
HiTrap® Heparin High Performance column	Cytiva	17040701
HiLoad Superdex 200 pg column	Cytiva	28989335
Typhoon RGB Biomolecular Imager	Cytiva	28-9969-43
Quantstudio 5 RT-PCR System	Thermo Fisher Scientific	A34322
StepOnePlus™ Real-Time PCR System	Applied Biosystems	4376600
Leica TCS SP5 II	Leica	DMI6000 CS

RESOURCE AVAILABILITY

Lead contact

Further information and requests for resources and reagents should be directed to the lead contact, Lynne E. Maquat (Lynne_Maquat@URMC.Rochester.edu).

Materials availability

Unique reagents generated for this paper are listed in the key resources table. Reagent requests should be directed to the lead contact.

Data and code availability

- All data reported in this paper are included in the supplemental tables. Requests for further information should be directed to the lead contact.
- This paper does not report original code.
- Any additional information required to reanalyze the data reported in this paper is available from the lead contact upon request.

EXPERIMENTAL MODEL AND SUBJECT DETAILS

Cell lines

HAP1 cells (male), HEK293T cells (female), and CVB and *FMR1*-KO iPSCs and neuronal stem cells (male) were all cultured at 37°C and in 5% CO_2 in various growth conditions depending on cell line and experimental design. A detailed description of all cell culture conditions for each cell line is provided in method details.

METHOD DETAILS

Plasmid constructions

Plasmids encoding 3XFLAG-mCherry, either with (+) or without (Δ) the JC intron, and HA-mCerulean were constructed as previously described (Popp and Maquat, 2015) with the following clarifications. Briefly, 3XFLAG-mCherry was PCR-amplified from pmCherry-C1 (Clontech) using the primer pair 5'-AAAGATCATGACATCGATTACAAGGATGACGATGACAAGGGCGGAGGTATGGTGAGCAAG-3' (sense) and 5'-CGTATAATGTATGCTATACGAAGTTATATCAGTCAGTCACTTGTACAGCTCGTCCAGCC-3' (antisense). The resulting PCR product was subjected to a second round of PCR using the primer pair 5'-GCATGCATGGGCCCGCCACCATGGACTACAAAGACCATGACGGTGATTAT AAAGATCATGACATCGATTACAAGGATGACGATG-3' (sense) and 5'-GTACCCATCAGGGATATCTCCTTTCTCCGTGCTGTCAGCGAC*ATAACTTCGTATAATGTATGCTATACGAAGTTAT*ATCAGTCAGT-3' (antisense; here and below, nucleotides in italics and underlined specify LoxP sites) to obtain the 3XFLAG-mCherry fragment. The +(JC Intron) and Δ(JC Intron) 3'UTR fragments were amplified from the described plasmids (Paillusson et al., 2005) using the primer pair 5'-CGGAGAAAGGAGATATCCCTGATGGGTAC-3' (sense) and 5'-CTTCGTATAATGTATGCTATACGAAGTTATTCAACGAGGAAGGTGGTCAGGG-3' (antisense), and each fragment was used as template in a second round of PCR using the primer set 5'-CGGAGAAAGGAGATATCCCTGATGGGTAC-3' (sense) and 5'-GCATGCGGGCCC*ATAACTTCGTATAATGTATGCTATACGAAGTTAT*TCAACGAGG-3' (antisense). The resultant fragments were fused to the 3XFLAG-mCherry fragment using standard overlap extension PCR and the primer pair 5'-GCATGCATGGGCCCGCCACCATGGACTACAAAGACCATGACGGTGATTATAAAGATCATGACATCGATTACAAGGATGACGATG-3' (sense) and 5'-GCATGCGGGCCC*ATAACTTCGTATAATGTATGCTATACGAAGTTAT*TCAACGAGG-3' (antisense). PCR products were digested with ApaI (NEB) and inserted into a similarly digested bidirectional lentiviral vector containing HA-mCerulean to yield the final reporter plasmids.

GI and MUP plasmids (Popp and Maquat, 2015), the YFP-GPx1 Norm and Ter reporter plasmids [gifts from Fabrice Lejeune (Palma et al., 2021)], and the MYC-UPF1 expression vectors (Hwang et al., 2010) have been previously described.

Please cite this article in press as: Cho et al., AKT constitutes a signal-promoted alternative exon-junction complex that regulates nonsense-mediated mRNA decay, Molecular Cell (2022), https://doi.org/10.1016/j.molcel.2022.05.013

To construct pCMV-MYC-UPF1^{R} (T151D), a 5'-fragment of UPF1 cDNA was PCR-amplified using pCMV-MYC-UPF1^{R} (Isken et al., 2008), Phusion DNA Polymerase (New England Biolabs), and the primer pair 5'-GAGGCGTACGGGCCCAGCTC-3' (sense) and 5'-GTGGCTGCCAGAA**TC**ATTTCCACGTC-3' (antisense). A 3'-fragment of UPF1 cDNA was likewise PCR-amplified using the primer pair 5'- GACGTGGAAAT**GA**TTCTGGCAGCCAC-3' (sense) and 5'-GCCCGGTACCGCTTCTCGTCG-3' (antisense). Bold nucleotides specify the mutations that introduce T151D, and underlined nucleotides specify BsiWI and KpnI sites, respectively. The resulting two PCR fragments were mixed and amplified using the sense oligonucleotide used to amplify the 5'-fragment and the antisense oligonucleotide used to amplify the 3'-fragment. The resulting PCR product was digested with BsiWI and KpnI and then ligated using T4 DNA ligase (Takara Bio) to replace the corresponding region of pCMV-MYC-UPF1^{R}. pCMV-MYC-UPF1^{R} (T151A) was identically constructed but using the primer pair 5'-GAGGCGTACGGGCCCAGCTC-3' (sense) and 5'- GTGGCTGCCAGAAG**C**ATTTCCACGTC -3' (antisense) to amplify the 5'-fragment of UPF1, and the primer pair 5'-GACGTGGAAAT**G**CTTCTGGCAGCCAC-3' (sense) and 5'-GCCCGGTACCGCTTCTCGTCG-3' (antisense) to amplify the 3'-fragment of *UPF1* cDNA.

Bacterial expression vectors for 6xHis-TEV-UPF1(115-914) WT, 6xHis-TEV-(115-914) T151D, and 6xHis-TEV-UPF1(115-914) T151A were generated using ligation-independent cloning into the pMCSG7 vector (a gift from Jeanne Stuckey, University of Michigan) as previously described (Eschenfeldt et al., 2009). Briefly, PCR amplification of the UPF1(115-914) inserts was performed using each pCMV-MYC-UPF1 variant, Phusion DNA Polymerase, and the primer pair: 5'-TACTTCCAATCCAATGCCACGAAGGACCTCCC CATACACGC-3' (sense) and 5'-TTATCCACTTCCAATGTTAGAGCGGCCCCTCCACCAG-3'(antisense). Each insert was then incubated on ice for 30 min with pMCSG7, which had been digested with SspI and then incubated with T4 DNA Polymerase in the presence of only dGTP to generate 15-bp overhangs, and used to transform DH5α competent cells.

Cells and cell culture for the haploid genetic screen

Near-haploid HAP1 cells (Carette et al., 2010) were cultivated in Iscove's Modified Dulbecco's Medium (Gibco) supplemented with 1x GlutaMAX (Gibco) and 10% FBS (Gibco). HEK293T cells (ATCC) for gene trap retrovirus production were cultivated in DMEM (Gibco) with 10% FBS.

Virus production, cell infection, and FACS sorting for the haploid genetic screen

For production of lentivirus, Lenti-X HEK293T cells (Clontech) were used with Lenti-X VSV-G packaging single shots (Clontech) according to manufacturer's directions. Infected HAP1 cells were selected with Zeocin (200 mg/mL; Gibco), followed by single-cell sorting into a 96-well plate using an LSR-II flow cytometer (BD Biosciences). Colonies were expanded, split into two plates, and then one plate was infected with Ad5CMV-Cre virus (University of Iowa Gene Transfer Vector Core) at an MOI of 10. 3XFLAG-mCherry and HA-mCerulean fluorescence of infected and mock-infected cells was recorded using an LSR-II flow cytometer, and colonies displaying a large increase in fluorescence after infection were further expanded and subjected to another round of screening by infection with Ad5CMV-Cre.

For production of eGFP gene-trap retrovirus (Carette et al., 2009), producer HEK293T cells were cultured in DMEM supplemented with 30% FBS and plated into T-175 flasks 16-hours before transfection such that they were 80% confluent at transfection. Twelve flasks were used per virus preparation. For each flask, cells were transfected with 6.02 μg pCG-GAG/Pol (a gift from Sarah Loerch and Clara Kielkopf; (Ulm et al., 2007), 1.4 μg pCMV-VSV-G, 0.84 μg pAdvantage (Promega Corporation), and 2.2 μg each of pGT GFP (0), 2.2 μg pGT GFP (+1), and 2.2 μg pGT GFP (+2) (Carette et al., 2009) using 45 μL Turbofectin 8.0 (Origene) in 850 μL OptiMEM (Gibco). Viral supernatants were harvested at 40 hours and then every 24-hours thereafter for a total of four harvests. Virus was pelleted by ultracentrifugation in an SW-28 rotor (Beckman) at 21,000 rpm for 2 hours at 4 °C. Viral pellets were resuspended in a minimal amount of Hanks Balanced Salt Solution (HBSS, Gibco). Sixty million P9_9_E12 HAP1 cells were plated at 7.5x10^{6} cells/15-cm dish 24-hours before infection with the gene-trap retrovirus. For infection, concentrated viral supernatant was applied to cells with 10 mg/mL protamine sulfate (MP Biomedicals). Infection was performed 4 times at 24-hour intervals. Infected cells were then frozen at 10x10^{6} cells/vial for temporary storage at -80°C.

Infected cells were then subjected to FACS sorting using the LSR-II flow cytometer to isolate the top 1-3% of 3XFLAG-mCherry-expressing cells. Cells (10x10^{6}) were isolated in this way, expanded for several passages, and subjected to a second round of FACS sorting.

Flow cytometry for the haploid genetic screen

Analytical flow cytometry was performed on an 18-Color LSR-II instrument (BD Biosciences), recording excitation from a Green 532 nm laser with a 610/20 nm band-pass filter (3XFLAG-mCherry fluorescence), and from a Violet 407 nm laser with a 450/50 nm band-pass filter (HA-mCerulean fluorescence). Cell sorting and capture was performed on a FACS AriaII instrument (BD Biosciences) using similar parameters and gating to capture the top 1-3% 3XFLAG-mCherry-expressing cells. Captured cells were then immediately plated and incubated to allow for recovery.

Linear-amplification-mediated (LAM)-PCR and sequencing for the haploid genetic screen

LAM-PCR was performed essentially as described (Brockmann et al., 2017), with the following additional details. Genomic DNA from 10 million sorted and 10 million unsorted control cells was isolated using a QIAamp DNA Mini Kit (Qiagen) according to manufacturer's directions, except elution was performed using 110 μL of H_2O after a 15-minute incubation at 37 °C. This was done twice,

followed by elution using 60 μL of H_2O and a 15-minute incubation for a total of 270 μL of genomic DNA at a concentration of ~200 ng/μL. Sixteen LAM-PCR reactions for each population (sorted and control unsorted) were performed, with 2 μg of input DNA each and 0.375 pmol of double-biotinylated (5'-double biotin-GGTCTCCAAATCTCGGTGGTGGAAC-3') primer per reaction (Brockmann et al., 2017).

PCR reactions were pooled (two LAM-PCR reactions per tube), and biotinylated DNA was purified using 20 μL of M-270 Streptavidin-coupled Dynabeads (Thermo Fisher Scientific), non-stick RNase-free microfuge tubes (Ambion), and 1:1 volume of 2x Lithium Binding Buffer (6 M LiCl, 10 mM Tris, 1 mM EDTA, pH 7.5). Binding was performed at 4 °C overnight, followed by four washes with 800 μL of Phosphate Buffered Saline (PBS) and 0.05% Triton X-100.

Linker ligation to the 3' end of the resulting PCR products was performed using Circligase II (Lucigen) exactly as described (Brockmann et al., 2017). Beads were then washed four times with 800 μL of PBS and 0.05% Triton X-100.

For the second, exponential PCR reaction, beads containing two LAM-PCR reactions per tube (i.e., one linker ligation reaction) were used for one exponential PCR reaction. PCR was performed exactly as described (Brockmann et al., 2017). PCR reaction supernatants were analyzed in a 1% agarose gel, then separately purified using a QIAquick PCR Purification Kit (Qiagen). Reactions showing homogenous smears only were pooled and submitted for sequencing on a HiSeq2500 instrument (Illumina) as described (Brockmann et al., 2017). Sequencing was performed by the University of Rochester Functional Genomics Center. Data were analyzed using a standard pipeline available at https://github.com/BrummelkampResearch.

Steady-state NMD reporter assays of candidate NMD effectors identified in the haploid genetic screen

HEK293T cells grown in DMEM supplemented with 10% FBS were plated at 41,570 cells per well of a 24-well plate 24-hours before transfection. Cells were then transfected with 12.31 pmol per well of CTL#1 siRNA (Ambion), CTL#2 siRNA (Sigma) or siRNA to a cellular protein (Dharmacon) using 0.616 μL RNAiMAX. Cells were transfected 24-hours later with either 17.687 ng of the Gl Norm test plasmid or Gl Ter and 7.075 ng of the MUP reference plasmid. After 24 hours, cells were harvested. RNA was extracted and subjected to RT-qPCR as described (see below).

NMD reporter mRNA half-life assay of candidate NMD effectors identified in the haploid genetic screen

HEK293 Tet-OFF Advanced cells (Clontech) were plated at 20,785 cells per well of a 48-well dish in 250 mL of DMEM supplemented with 10% FBS and incubated overnight. The next morning, cells were transfected with siRNA using a mixture of 53 μL OptiMEM (Thermo Fisher Scientific), 0.3 μL RNAiMAX, and 0.063 μL of 100 μM siRNA per well and incubated for 24 hours. Cells were subsequently transfected with a mixture of 15 ng of either human Gl Norm Tet-OFF or human Gl Ter Tet-OFF plasmid (Popp and Maquat, 2015) and 10 ng of MUP plasmid, in 12.5 μL Opti-MEM with 0.125 mL Lipofectamine 2000 (Thermo Fisher Scientific). Cells were allowed to recover for 48 hours, after which cells were incubated with 50 mg/mL doxycycline (Sigma Aldrich, ready-made solution) and harvested at the indicated times.

HEK293T cells and cell culture after verification of effectors identified in the haploid genetic screen, including mRNA half-life studies

HEK293T cells (ATCC), which were cultivated in DMEM (Gibco) with 10% FBS, were transfected with siRNA using RNAiMAX (Thermo Fisher Scientific), and/or plasmid using Lipofectamine 2000 (Thermo Fisher Scientific). Unless noted otherwise, test plasmids encode FLAG-Gl Norm or FLAG-Gl Ter mRNA (Kurosaki et al., 2021a), and the reference plasmid encodes MUP mRNA. When specified, cells were cultured in the presence of 600 nM afuresertib (Afu; Selleckchem, GSK2110183) in DMSO (VWR) or DMSO alone. In other experiments cells were serum-starved for 24-hours followed by incubation without or with 100 nM insulin (Thermo Fisher Scientific) for 30-min.

Generation and use of *FMR1*-KO iPSC line

The *FMR1*-KO iPSC line was generated by nucleofecting the parental CVB cell line (Coriell GM25430) according to Lonza's Nucleofector-2B program B-016 with 2 plasmids encoding two small guide RNAs (see key resources table) targeting an overlapping region (5'-GTTGGTGGTTAGCTA-3') of *FMR1* exon 4. *FMR1*-KO cells harbor a 19-bp deletion in exon 4 (5'-TTGCTGTTGGTGGTTAGCT-3'). This deletion, analyzed by Sanger sequencing, generates a nonsense codon between codons 77 and 78, loss of FMRP as verified by western blotting (e.g. Figure 5A), and an otherwise healthy and stable karyotype (Table S8), consistent with the selective introduction of this frameshift mutation that results in a nonsense codon in *FMR1* mRNA.

iPSCs were differentiated to NSCs using dual-Smad-inhibition (Chambers et al., 2009; Qi et al., 2017). Briefly, iPSCs cultured in StemFlex (Thermo Fisher Scientific) on Matrigel (Corning Life Sciences) were dissociated into single cells using Accutase (Stem Cell Technologies) and plated ($5x10^4$ cells/cm^2) on Matrigel-coated plates in the presence of ROCK inhibitor Y27632 (HelloBio). The following day, the medium was changed to E6 Medium (Thermo Fisher Scientific) containing the Smad inhibitors SB431542 (Cayman Chemicals) and LDN-193189 (Cayman Chemicals), and the tankyrase inhibitor XAV939 (Tocris). Following daily medium changes for 5 days, cells were transitioned to DMEM/F12 (Gibco) containing N-2 and B27 (Thermo Fisher Scientific) and supplemented with Epidermal growth factor (EGF; PeproTech), Fibroblast growth factor-2 (FGF-2; Miltentyi Biotec), LDN-193189, and CHIR-99021 (MedChem Express) for expansion. NSCs were further purified through positive selection for expression of CD15 using anti-CD15 microbeads (Miltenyi Biotec) (Capela and Temple, 2002; Pruszak et al., 2009).

Please cite this article in press as: Cho et al., AKT constitutes a signal-promoted alternative exon-junction complex that regulates nonsense-mediated mRNA decay, Molecular Cell (2022), https://doi.org/10.1016/j.molcel.2022.05.013

NSCs were characterized by expression of neural stem-cell markers PAX6, SOX1, HES5, ZIC1, Nestin (Chambers et al., 2009), MSI1 (Dhara et al., 2008), Vimentin (Reubinoff et al., 2001), and SOX2 (Ellis et al., 2004), using immunofluorescent (IF) antibody-labeling and RT-qPCR. NSCs for IF labeling were plated on Matrigel-coated glass coverslips. Cells were fixed with 4% w/v paraformaldehyde (MP Biomedicals) in PBS, permeabilized with 0.5% v/v Triton X-100 (Sigma Aldrich) and blocked and stained with 10% goat serum (EMD Millipore), 1% bovine serum albumin (Lee BioSolutions), and 0.2% Triton-X 100 in PBS. Antibodies and dilutions are listed in key resources table. Images were acquired using a Leica TCS SP5 II confocal laser-scanning microscope, and montages were assembled using Leica LASAF and Image J (Fiji, Version 2.1.0). RT-qPCR analyses were performed using total-cell RNA that was isolated from ~1x10^6 cells using TRIzol reagent (Thermo Fisher Scientific). Purified RNA was treated with RNase-free DNase I, reverse-transcribed using random primers and Superscript III, and amplified using hydrolysis qPCR probes (see key resources table) with Amplitaq DNA Polymerase on a Quantstudio 5 real time PCR system (all Thermo Fisher Scientific). The ΔΔCt method (Livak and Schmittgen, 2001) was used to determine the relative gene expression levels, normalized to mRNA encoding the TATA-binding protein (Augustyniak et al., 2019).

For assaying NMD activity, cells were plated at 2x10^4 cells/cm^2 and maintained in DMEM/F12 containing N-2 and B27 and supplemented with EGF and FGF-2, in the absence of LDN-193189 and CHIR-99021. NSCs were cultured with 600 nM Afu in DMSO for the indicated times and lysed in hypotonic lysis buffer (Kurosaki et al., 2014) without subsequent sonication.

siRNA sequences

UPF1 and *SMG1* siRNAs were as previously described (Kurosaki et al., 2014; Popp and Maquat, 2015). All siRNA commercial sources and/or sequences are listed in the key resources table.

Western blotting

Proteins in cell lysates were electrophoresed in 8% polyacrylamide and subjected to western blotting as described (Popp and Maquat, 2015) using antibodies listed in the key resources table.

Immunoprecipitations

HEK293T cells were washed with ice-cold PBS. Cells were harvested and suspended in the Hypotonic Gentle Lysis Buffer (10 mM Tris pH 7.5, 10 mM NaCl, 10 mM EDTA, 1% [w/w] Triton X-100) with protease inhibitor cocktail (Roche). The NaCl concentration was adjusted to 150 mM followed by clarification of cell lysates at 16,000xg for 10 min. IPs were performed as previously described (Cho et al., 2012; Kurosaki et al., 2014) using 5 μg of antibody (see key resources table) pre-bound to 50 μL of Protein A Agarose (Roche) or 50 μL of α-MYC magnetic beads (Thermo Fisher Scientific). Antibody-bound beads were incubated with cell lysates, washed twice with NET2 Buffer (50 mM Tris-HCl pH 7.4, 150 mM NaCl, 0.05% NP-40, 1× HaltTM Protease and Phosphatase Inhibitor Cocktail EDTA-Free), treated for 10 min at 37°C with RNase ONE (Promega). Beads were washed 5-10 times using NET2 buffer, and complexes were eluted using 2× SDS sample buffer and split into two portions. One portion was used as a source of protein, which was analyzed by SDS-PAGE and Western blotting. The other portion was extracted with TRIzol reagent (Life Technologies) followed by ethanol precipitation and used as a source of RNA for RT-qPCR.

RNA purification and RT-qPCR

RNA was extracted from cell lysates before or after IP using TRIzol (Thermo Fisher Scientific) according to the manufacturer instructions and subjected to RT-qPCR as described (Popp and Maquat, 2015). Briefly, RNA was treated with 2 μL of RQ1 DNase (Promega) at 37°C for 45 min, extracted using phenol-chloroform, and ethanol precipitated. cDNA was synthesized using 200 ng of RNA and SuperScript III Reverse Transcriptase (Thermo Fisher Scientific) according to manufacturer instructions. RT-qPCR was performed using a set of forward and reverse gene-specific primers at 0.8 μM each (see Table S5). For qPCR performed using Fast SYBR Green Master Mix (Applied Biosystems) and the StepOnePlus™ Real-Time PCR System (Applied Biosystems), the following cycling conditions were employed: one cycle at 95°C for 10 sec, followed by 40 cycles where each cycle consisted of 95°C for 15 sec and then 60°C for 1 min. For qPCR performed using PerfeCTa SYBR Green SuperMix, Low ROX (Quantabio) and the 384-well QuantStudio 5 Real-Time PCR System (Applied Biosystems), the following cycling conditions were employed: one cycle that consisted of 50°C for 2 min and then 95°C for 10 min, and subsequently 40 cycles, where each cycle consisted of 95°C for 15 sec and then 60°C for 1 min.

Mapping UPF1 phosphorylation sites using mass spectrometry

Baculovirus stocks for the expression of FLAG-tagged human UPF1 were generated as previously described (Bhattacharya et al., 2000; Hosoda et al., 2005). Briefly, Sf9 insect cells were transfected with pBacPAK8-FLAG-UPF1 and Bsu36 I-digested pBacPAK6 plasmids using Bacfectin (Takara Biosciences). Five days post-transfection, baculovirus was harvested. A clonal viral stock was produced from a single viral plaque to ensure that only recombinant virus producing FLAG-UPF1 was used to generate FLAG-UPF1 protein. Viral titers were measured using the BacPAK Baculovirus Rapid Titer Kit (Takara Biosciences). For FLAG-UPF1 production, ~10x10^6 Sf9 cells grown in a monolayer on a 15-cm plate were infected at an MOI of 4. Three days later, cells were incubated with or without 200 nM okadaic acid (LC Laboratories) for 2−3 hours and subsequently lysed in 20 mM Tris, pH 7.5, 500 mM NaCl, 20 mM β-glycerophosphate, 1 mM EDTA, and 1x Complete Protease Inhibitor Cocktail (Roche) (Isken et al., 2008). FLAG-UPF1 was

Please cite this article in press as: Cho et al., AKT constitutes a signal-promoted alternative exon-junction complex that regulates nonsense-mediated mRNA decay, Molecular Cell (2022), https://doi.org/10.1016/j.molcel.2022.05.013

affinity purified using M2-FLAG affinity resin (Sigma) (Bhattacharya et al., 2000; Hosoda et al., 2005) and dialyzed into 20 mM ammonium bicarbonate prior to proteolytic digestion with trypsin (Promega), chymotrypsin (Pierce), and Glu-C (Pierce), either individually or in combination. LC-MS/MS analyses were performed by the University of Rochester Mass Spectrometry Resource Lab.

Purification of UPF1 variants from *E. coli*

UPF1 variant purification was performed by the University of Michigan Center for Structural Biology following a modified protocol (Chakrabarti et al., 2011). pMCSG7 vectors expressing 6xHis-TEV-UPF1(115-914) WT, T151D, and T151A were introduced into Rosetta 2 (DE3) cells (Novagen). Transformed cells were expanded in Terrific Broth (24 g/L yeast extract, 20 g/L tryptone, 4 mL/L glycerol, 0.017 M KH_2PO_4, 0.072 M K_2HPO_4) supplemented with ampicillin (100 μg/mL) at 18 °C overnight and then lysed in the presence of DNase I (Sigma) and 1mM PMSF (Sigma). UPF1 variants were purified from the resulting lysates using, sequentially, Ni^{2+}-affinity chromatography (Qiagen), ion exchange using heparin sulfate (Cytiva Life Sciences), and size exclusion using Superdex 200 (Cytiva Life Sciences). Purified proteins were concentrated to 5 mg/mL and flash frozen.

In vitro kinase, helicase, ATPase, and RNA-binding assays

All assays used WT, T151D or T151A variants of UPF1(115-914). In kinase assays, each variant (1 μg) was incubated at room temperature for 1-hour with 0, 50, or 100 ng of AKT1, AKT2, or AKT3 (all from Promega Corporation) using the AKT Kinase Enzyme System (Promega Corporation). UPF1, AKT, and AKT-mediated phosphorylation of UPF1 were detected using Western blotting.

Helicase assays were as previously described (Chakrabarti et al., 2011; Kurosaki et al., 2014). Briefly, for the RNA:DNA duplex, a 44-nt RNA was synthesized using the MEGAscript T7 Transcription Kit (Invitrogen) and a T7 promoter-containing DNA duplex (5'-GGATCCTAATACGACTCACTATAG**GGGCGAATTCAAAACAAAACAAAACTAGC ACCGTAAAGCAAGCT**-3', sense strand, *in vitro*-transcribed region in bold; IDT), purified using the RNA Clean and Concentrator Kit (Zymo Research), and annealed to a 5'-Cy3-labeled 18-nt single-stranded DNA (5'-Cy3-AGCTTGCTTTACGGTGCT-3'; IDT). Duplexes were purified from 12% polyacrylamide using the ZR small-RNA PAGE Recovery Kit (Zymo Research). Each UPF1 variant (50 and 100 ng) was incubated at 37 °C for 30 min with 20 nM RNA:DNA duplex in the absence or presence of 2 mM rATP (Promega). Reactions were resolved in a 10% native polyacrylamide gel and imaged using a Typhoon RGB biomolecular imager.

ATPase assays were performed essentially as described (Kurosaki et al., 2014) using 75 ng of each UPF1 variant.

RNA-binding assays were performed by incubating increasing amounts of each UPF1 variant (0−150 μM) at room temperature for 30 min with 1 nM 5'-Cy3-RNA (5'-Cy3-GGGCGAAUUCAAAACAAAACAAAACUAGCACCGUAAAGCAAGCU-3'; IDT) in UPF1 Helicase Buffer lacking ATP (Chakrabarti et al., 2014). Binding reactions were resolved in a 6.5% native polyacrylamide gel and imaged using a Typhoon RGB biomolecular imager.

The relative activity of each AKT paralog was assessed using the AKT Kinase Enzyme System and ADP-Glo Luciferase Assay (Promega Corporation) per the manufacturer instructions. Briefly, 100 ng of each AKT paralog were reacted with 0.2 μg/μL modified AKT substrate derived from the N-terminus of GSK3β (modified-CKRPRAASFAE; SignalChem) and 150 μM rATP (Promega Corporation).

QUANTIFICATION AND STATISTICAL ANALYSIS

For the haploid genetic screen, data analyses and significance cutoffs are described in results and in Tables S1–S4. Microsoft Excel was used to perform the statistical analyses specified in figures, figure legends, and tables. For all experiments, standard curves were generated to ensure that all measurements fall within a linear range of analysis for the indicated antibody (for western blots), primer set (for RT-qPCR), and fluorescent oligonucleotide (for helicase and RNA-binding assays). For RT-qPCR experiments, histograms represent the mean of three measurements from biological replicates, and error bars represent standard deviations. Significance cutoffs for P values were defined as (*) $P < 0.05$ and (**) $P < 0.01$. P-values were calculated using a two-tailed unpaired Student's *t*-test, except for the RT-qPCR experiments performed in Figures S5C–S5H, which used a one-tailed Student's *t*-test. For mass spectrometry analyses, high-confidence phosphorylation sites were defined as those sites with a Mascot score >15 and a ΔM/z between -0.8 and +0.5. In densitometric analyses, gels showing the results of helicase and RNA-binding assays were quantitated using ImageQuant (Cytiva), and western blot results were quantitated using ImageLab (BioRad). Quantitations are representative of results obtained from 2 or 3 independent experiments, as indicated in figure legends.